Coordination Chemistry Reviews 359 (2018) 32–51

Contents lists available at ScienceDirect

Coordination Chemistry Reviews

journal homepage: www.elsevier.com/locate/ccr

Review

Emerging nanomaterials with advanced drug delivery functions; focused on methotrexate delivery

Goeun Choi [a], Tae-Hyun Kim [b], Jae-Min Oh [b], Jin-Ho Choy [a,*]

[a] Center for Intelligent Nano-Bio Materials (CINBM), Department of Chemistry and Nano Science, Ewha Womans University, Seoul 03760, Republic of Korea
[b] Department of Chemistry & Medical Chemistry, College of Science & Technology, Yonsei University, Wonju, Gangwon-do 26493, Republic of Korea

ARTICLE INFO

Article history:
Received 25 October 2017
Accepted 5 January 2018

Keywords:
Drug delivery
Nanovehicles
Methotrexate
Layered double hydroxides
Chemotherapy

ABSTRACT

This review focuses on therapeutic applications of various drug delivery nanovehicles encapsulated with the anti-cancer drug, methotrexate (MTX). Currently, a number of studies have been conducted to explore advanced chemotherapeutic systems with nonviral nanovehicles such as liposomes, polymeric micelles, polymersomes, solid lipids, dendrimers, porous metal and metal oxide particles, carbons with various nanostructures, and layered double hydroxides (LDHs). Out of various anticancer drugs, MTX was hybridized with those drug delivery nanovehicles not only to overcome its adverse effects, but also to induce advanced functions into those hybrid systems, such as enhanced solubility, controlled release, passive and active targeting, aimed to eventually enhance bioavailability of MTX. In particular, two dimensional LDHs are introduced rather in detail as one family of inorganic nanovehicles, since the therapeutic efficacies for MTX-LDHs have been systematically studied with *in vivo* orthotopic models, those which are clinically better correlated and therefore, more efficient to predict drug efficacy and toxicity than the standard one like xenograft model. Attempts are also made here to provide therapeutic results on chemically well defined MTX-LDH advanced drug delivery systems, such as their *in vitro* and *in vivo* targeting functions, biocompatibility and nanotoxicities and ability to overcome drug resistance. In addition, recent advances and challenges in advanced hybrid DDSs are discussed from the viewpoint of state-of-the-art nanomedicine.

Contents

* Corresponding author.
E-mail address: jhchoy@ewha.ac.kr (J.-H. Choy).

https://doi.org/10.1016/j.ccr.2018.01.007
0010-8545/

1. Introduction

Many attempts are being made to maintain better quality of life and well-being of our society. In particular, medical technology, therapeutics and diagnostics have made remarkable advances, but they should be less costly and burdensome without increasing care services. More recently, efforts have been made to advance nanotechnolgy in terms of novel drug delivery systems with advanced properties that encapsulate conventional chemotherapeutic agents into functional nanovehicles. And therefore, scientists in the medical community have achieved nanomedicine as a breakthrough in the fight against cancer. According to the European Technology Platform Document, nanomedicine can be defined as a medicine using nanotechnology, which is composed of approximately six research fields including drug delivery, biomaterials, *in vitro* diagnostics, drugs and therapies, *in vivo* imaging, and active implants [1,2]. However, drug delivery is thought to be the most significantly studied from the six research fields according to the total number of papers published and patents filed worldwide [3].

To exploit nanosized drug delivery systems (nDDSs), development of new drug delivery nanovehicles with desired properties such as high drug-loading concentration, controllable therapeutic windows, excellent targeting functions, and low toxicity is required. The biggest advantage of DDSs is surely due to therapeutic window control. As shown in Fig. 1, the therapeutic window is defined as the efficacy level of drug concentration by the time between diminished activity and toxic levels. In most drug administrations, it is challenging to maintain the appropriate therapeutic level in terms of plasma concentration, and therefore, repeated administrations are often required, resulting in drug resistance, toxicity scares and eventually inconvenience to patients. However, controlling the therapeutic window through DDS with sustained release functions allows drug efficacy to be maintained at the required plasma concentrations with a single drug administration, which can subsequently lead to minimizing the previously mentioned disadvantages and side effects due to repeated administrations.

Methotrexate (MTX) is considered as one of the first generation anticancer drugs prescribed for human cancers such as osteosarcoma, leukemia, cervical and breast cancer, hematologic malignancies, and even rheumatoid arthritis [4,5]. Though clinical uses of MTX in cancer are well reported [6], its clinical efficacy can be restricted due to its very short plasma half-life, poor pharmacokinetics, susceptibility to development of patient drug resistance, and eventual high dosages required for chemotherapy [6,7].

In order to deliver MTX in an efficient way, many studies in the drug delivery community have been carried out, not only to improve drug efficacy and pharmacokinetics, circulation in the blood, controlled release and therapeutic window, but also to overcome drug resistance. It has further been suggested that the hybridization of MTX with nanocarriers could open new developments in nanomedicine. As shown in Fig. 2, various nonviral nanovehicles, such as inorganic and organic/polymers, are now available.

In this review, various studies highlighting recent advances in MTX hybridized with nanovehicles are presented from the viewpoint of DDSs in nanomedicine, along with the up-to-date issues related to such MTX-nanovehicle hybrids *in vitro* and *in vivo*. In particular, the inorganic nanovehicle, layered double hydroxide (LDH), is discussed in detail. In order to develop such drug delivery vehicles with the desired functions listed above, it is most essential to develop a biocompatible drug delivery carrier with passive and active targeting functions. Among various nanovehicles, the one most intensively studied in various animal models is the injectable nanohybrid DDS, MTX-LDHs. Out of them, the *in vivo* orthotopic model is thought to be clinically better correlated and as a consequence more efficient to predict drug efficacy and toxicity than the standard ones like subcutaneous models. Since tumor cells are implanted directly into the relevant organ, this model reflects real situations (such as tumor microenvironments) seen in cancer patients much more effectively than the conventional one like xenograft tumor model [8].

2. History of methotrexate

Methotrexate (MTX) as an anticancer drug, (2S)-2-[(4-{[(2,4-diamino-7,8-dihydropteridin-6-yl)methyl](methyl)amino}phenyl)form-

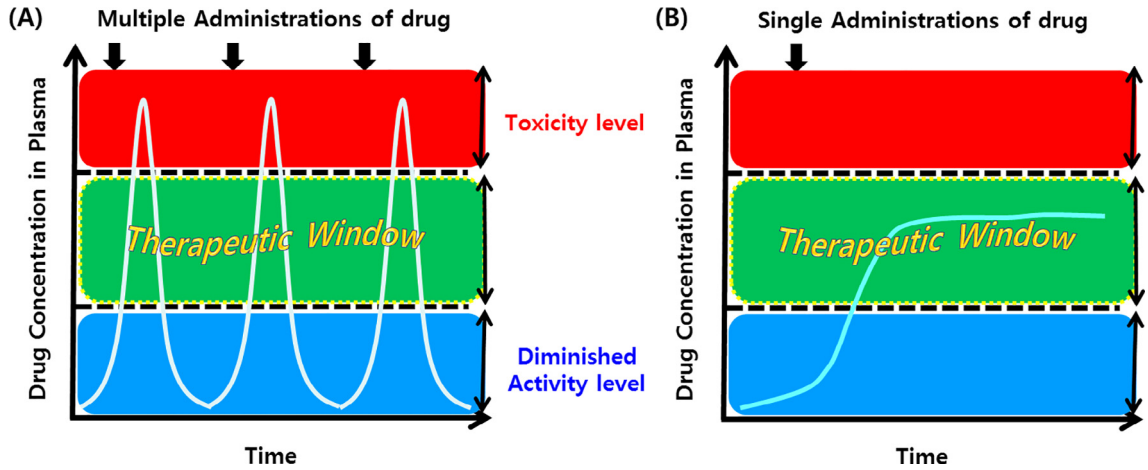

Fig. 1. Schematic diagram of therapeutic window with (A) multiple administrations of a conventional drug, and (B) single administration of drugs through a drug delivery system.

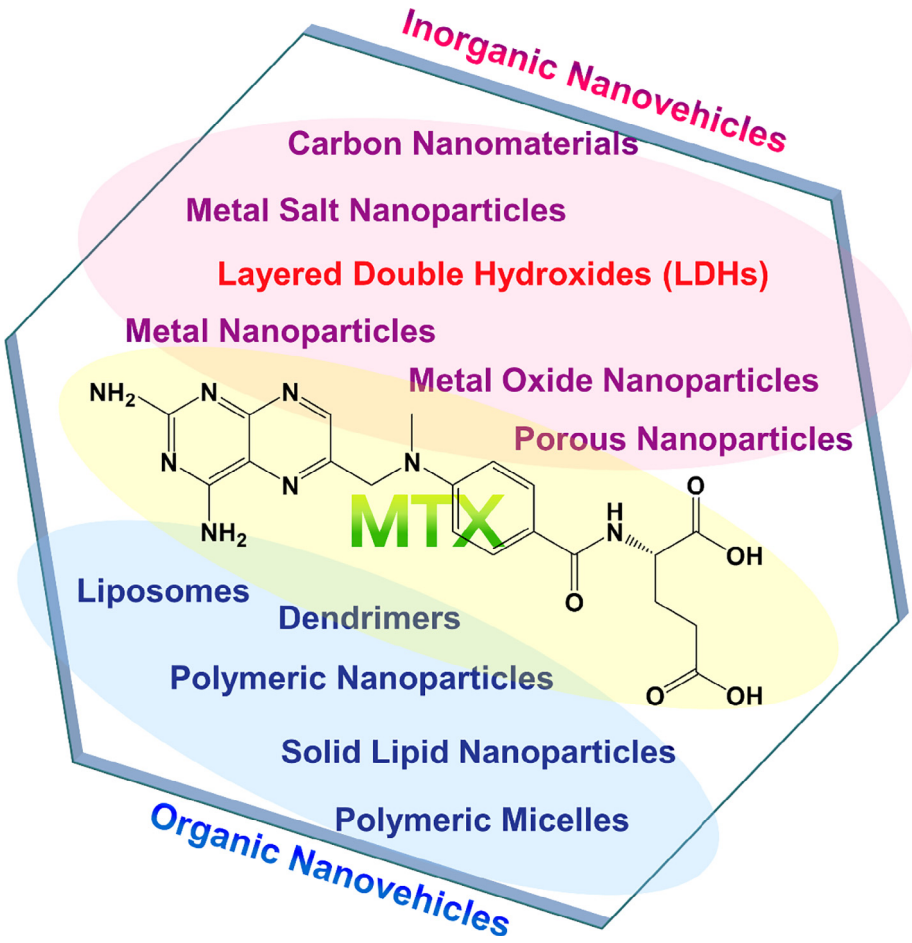

Fig. 2. Schematic diagram of methotrexate delivery nanovehicles classified into inorganic and organic materials.

amido]pen-tanedioi acid, was prepared for the first time by Seeger et al. about 70 years ago [5,9]. It is an analog of vitamin B_9 (folic acid) where the CH_3 and NH_2 groups are bonded to N10 and C4, respectively [5]. As shown in Fig. 3(A), the MTX molecule is consisted of three groups, namely, a pterin ring, p-aminobenzoic acid, and glutamate moieties [5,10]. The first results of preclinical and clinical researches made in 1956 demonstrated that the therapeutic efficacy of MTX was appeared to be better than that of aminopterin, which was discovered as a folic acid analog by Yellapragada Subbarao in 1947. In the same year, the efficacy of MTX in choriocarcinoma was established [6]. It was further explored for some types of cancer only with MTX and/or with other anticancer drugs, and was also extensively studied for other noncancer symptoms in the 1970s. In 1988 and 2002, the US Food and Drug Administration (FDA) approved this drug for the treatment of psoriasis, rheumatoid arthritis (RA) and Crohn's disease, respectively [6]. As an anticancer drug, MTX, was often utilized in the treatment of breast cancer based on combination therapy (CMF) with other anticancer agents, such as cyclophosphamide and 5-fluorouracil [11].

2.1. Advantages of methotrexate

In terms of intracellular cancer suppression mechanism, MTX has excellent strategy. As well represented in Fig. 3(B), once MTX is internalized inside cells, MTX molecules, as a folic acid (FA) antagonist, do form covalent bonds with the cytosolic enzyme, dihydrofolate reductase (DHFR), involved in the folate cycle. In this way, the folate cycle, coupled with thymidine and de novo DNA syntheses and cell proliferation, is stopped due to the deactivation of the intracellular enzymatic reaction from dihydrofolate to tetrahydrofolate, and as a consequence, the MTX permeation into the cytosol ultimately gives rise to cell death [12–16].

2.2. Disadvantages of methotrexate

In spite of excellent action mechanism in cancer cell suppression, the utility of methotrexate in cancer chemotherapy has been restricted due to unexpected adverse effects such as toxicity, low cellular influx, lack of cellular and systemic specificity, drug resistance and etc. Several examples of MTX's disadvantages are summarized below.

Michaels et al. studied the MTX treatment for rheumatoid arthritis (RA) patients via intravenous administration, where MTX was administered at weekly intervals with initial dose of 10 mg, but with a maximum dose of 50 mg for tolerant patients. Around 60–85% patients with high dose MTX have reported adverse drug reactions, and the 10–30% could not continue due to its toxicity [17]. In prospective studies, the 10–50% showed nausea, malaise and vomiting within 8 h after administration which continued for a few hours and up to one week [18]. Bertino et al. reported the MTX polyglutamate accumulated in intestinal mucosa cells, and observed gastrointestinal side effects [19]. As shown in the long-term prospective study of MTX by Kremer and Phelps, during 90 months of treatment, the 12–37% of RA patients showed side effects like stomatitis and mild alopecia, and only 4% of them asked for discontinuation of treatment [20].

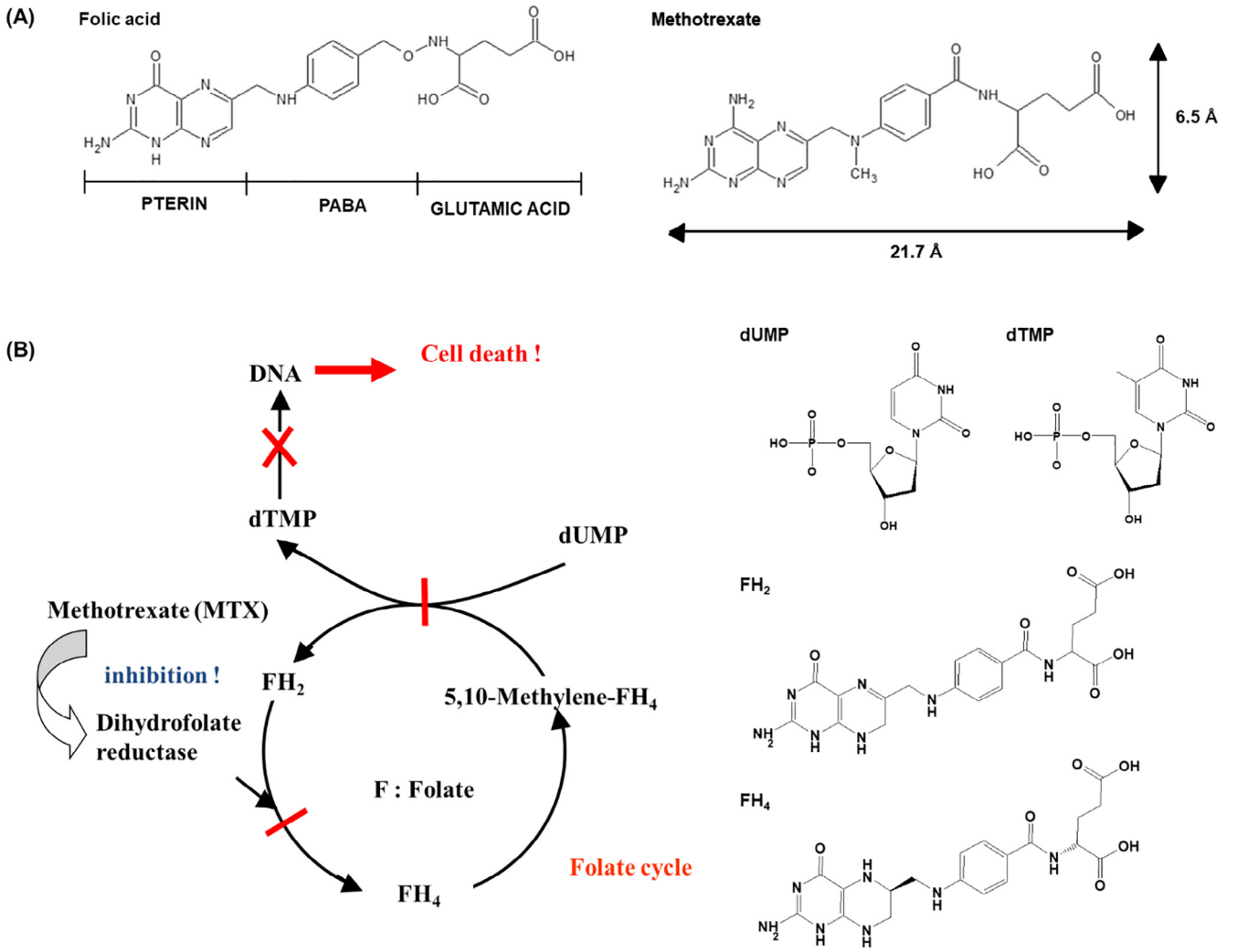

Fig. 3. (A) Molecular structure of folic acid and methotrexate. (B) The anticancer mechanism of methotrexate (MTX). Reproduced from Ref. [16] with permission of WILEY-VCH Verlag GmbH & Co. KGaA, Weinheim. (Abbreviations. dUMP: deoxyuridine monophosphate; dTMP: deoxythymidine monophosphate; FH_2: dihydrofolic acid; FH_4: tetrahydrofolic acid.)

After short term weekly MTX administration at higher doses, hematologic complications in RA patients have been reported infrequently; such side effects occurred in 2–3% of patients [17]. In a long-term study, the most frequent abnormality, such as leucopenia (8 patients) and thrombocytopenia (7 ones) could be observed from 271 RA patients [21]. According to Susan et al. the 7 cases of pancytopenia occurred out of 511 RA patients (1.4%) treated with low dose pulse MTX [22]. There were also some phenomena called the MTX side effects on the central nervous system, such as dizziness, headache, lightheadedness, vertigo, and mood alterations, from the 36% of patients as studied by Alarcóan et al. and Weinblatt et al. [23,24].

Liver toxicity in daily MTX treated patients was studied by Yazici et al. It was found that liver fibrosis, cirrhosis and psoriasis were formed from 24% of patients after increasing cumulative doses [25]. In the case of long-term weekly low-doses, MTX has not been associated with significant problems for RA patients. In general, however, the delayed excretion of MTX and its metabolites might result in toxicity to the kidneys and reproductive system, as demonstrated by Buckley et al. In particular, special care should be taken with pregnant patients, since multiple congenital abnormalities have been observed after weekly MTX treatments at a 10 mg dose during the first 3 months of pregnancy [26]. Some malformations were also reported due to MTX as reported by Furst et al. [27].

As described, a high dosage of MTX is unavoidable due to its short plasma half-life and very high rate of efflux relative to influx. MTX efflux is increased via ATP-binding cassette (ABC), which is the subfamily transporters such as ABCC1, ABCC2, ABCC3, ABCC4, ABCC5, and ABCG2 [14]. The MTX drug resistance can be obtained by upregulating drug-efflux proteins, which belongs to the multidrug-resistance transporters such as ABCs [28]. Many scientists, therefore, have attempted to hybridize MTX with nanocarriers to form hybridized MTX-nanocarriers to overcome these limitations.

3. Advanced drug delivery with nanovehicles

3.1. Organic nanovehicles

3.1.1. Liposomes

Liposomes are a self-assembly of amphiphile molecules and are commonly prepared with various lipid (phospholipids and cholesterol) bilayers with a membrane-containing water-soluble compartment and a hydrophobic one in and out of the bilayers [29]. Due to the characteristic internal and external surface structures, liposomes have been extensively investigated as drug/gene delivery vehicles. In general, drug molecules are immobilized in the core

Table 1
Summary of organic nanocarriers for methotrexate delivery.

Nanocarrier	Materials	Synthetic method	Encapsulation efficiency	Loading capacity	Release of MTX	IC_{50} value	Achievement	Reference
Liposome	γ-Fe_2O_3-glutamic acid and cholesterol	Reverse-phase evaporation method	61%	–	90% (41 °C, pH 5.5, 60 min)	–	3.8-fold and 9.7-fold higher values of C_{max} and AUC_{-0-t} than free MTX	Zhu [34]
	DSPE-PEG2000, DPPG, DSPC and PEG4000	Microbubble coupling method	83.4%	31.4%	–	–	3.6-fold higher MTX concentration in parietal lobe than free MTX	Wang [36]
	Ara-C and DPPC	Reverse-phase evaporation method	86%		21% (4 °C, pH 7.6, 28 d)	–	Sustained release of MTX even after 28 days	Pentak [37]
	PEG-P(HPMA-LA)-PDMA, Anis-PEG-P(HPMA-LA)-PDMA	Autocrosslinking method	65.1%	30%	20% (37 °C, pH 7.4, 24 h)	4.81 μM (H460)	100% survival rate after 45 days	Yang [38]
Polymeric Nanoparticle	Prot A7	Self-assembly method	52%	9.8%	100% (37 °C, pH 7, 80 min)	–	Sustained release at simulated gastric condition (pH 1.2)	Kumar [42]
	LHRH functionalized human serum albumin	Cross-linked by EDC	–	–	99% (4 °C, pH 7.4, 28 d)	5.82 nM (T47D)	Functionalized LHRH make it possible to internalized through LHRH receptor-mediated endocytosis	Taheri [43]
	Folic acid conjugated chitosan	Ionic corss-linking with TPP	–	11.5%	84% (37 °C, pH 6.8, 120 h)	–	Controllable MTX release through adjusting ratio of MTX and chitosan	Ji [44]
	Folic acid conjugated chitosan	Ionic corss-linking with TPP	89.6%	4.5%	65% (37 °C, pH 7.4, 72 h)	–	HeLa cells were successfully suppressed than free MTX	Beidokhti [45]
	PEGylated chitosan	Ion-induced combined with chemical cross-linking	87.7%	44.2%	5.5% (37 °C, pH 7.4, 144 h)	–	HeLa cells were 1.5-fold more inhibited than free MTX	Chen [47]
	Chitosan conjugated PAMAM	EDC coupling method	–	–	35% (37 °C, pH 7.4, 24 h)	0.36 μM (A549)	Higher cytotoxicity than free MTX (16 times)	Leng [48]
	Chitosan	Spray drying method	90.1%	–	75% (37 °C, pH 7.4, 3 h)	–	Higher brain uptake of MTX than free MTX	Sun [52]
	PLGA conjugated with positively charged bovine serum albumin	Solvent diffusion method	71.3%	–	20% (37 °C, pH 7.4, 8 h)	–	Highly tumor specific delivery across the BBB	Kesharwani [53]
Solid Lipid Nanoparticle	Stearic acid, soya lecithin and sodium taurodeoxycholate	Emulsion polymerization	40.9%	–	47.3% (37 °C, pH 7.4, 5 h)	–	Sustained release in mouse serum and extended half-life and MRT	Ruckmani [56]
	Hydrocarbonized porous silicon	Microfluidic flow-focusing method	12.5%	–	50% (37 °C, pH 7.4, 50 min)	–	Sustained release under various pH conditions	Liu [59]
	Imwitor, Neobee® Cremophor RH40 and Pluronic F127	High-shear homogenization method	70.3%	-	75% (37 °C, pH 7.4, 12 h)	0.013 μM (A2780)	Substantial suppression in proinflammatory and T-cell-derived cytokines	Abdelbary [60]
	Cetyl palmitate, Miglyol® 812 and polysorbate 80	Ultrasonication method	83%	–	56.9% (37 °C, pH 7.4, 24 h)	–	Increment of flux out MTX compared with free MTX (2-fold)	Ferreira [61]
	Stearic acid, Tween-80, soya lecithin and Triton X-100	Solvent diffusion method	22.3%	7.02%	55% (37 °C, pH 7.4, 48 h)	–	From *in vivo* biodistribution study with radioisotope labelled sample shows enhanced tumor uptake	Kakkar [62]
	Fucose, Pluronic F-68, Triton X-100 and Gelucire ® 50/13	Hot micro-emulsion method	84%	15.2%	85% (37 °C, pH 7.4, 96 h)	–	Surface modification with fucose enhance tumor targeting	Garg [63]
Polymeric micelle	mPEG–PLA	Polymerization at 150 °C for 16 h.	47.3%	12.8%	10% (37 °C, pH 7.4, 5 d)	–	Controlled release	Zhang [66]
	PEG-PLA	Thin-film hydration method	96.7%	9.6%	33% (37 °C, pH 7.4, 72 h)	0.76 μg/mL (KBv)	Controlled sustained release utilizing chain length of PLA	Chen [67]
	PEG-PCL	Polymerization under ring opening process	–	2.8%	80% (37 °C, pH 7.4, 6 h)	4 μg/mL (HeLa)	Structural engineering of diblock copolymer for multi drug loaded nanocarrier	Surnar [71]
	PLGA and soya lecithin	Emulsion	76.9%	30.6%	67.2% (37 °C, pH 7.4, 24 h)	–	Enhanced 4.9 times of half-life	Singh [72]
	PEG-CHO	Emulsion	32%	–	33% (37 °C, pH 7.4, 72 h)	–	pH and GSH responsive nanocarrier with high drug loading efficiency and controlled release	Duan [73]
Dendrimer	PAMAM and OEG	Dialysis method	85.2%	–	40% (37 °C, pH 7.4, 2 h)	8.9 μg/mL (MCF-7)	Good blood compatibility and high tumor growth inhibition	Zhao [76]
	Glucosamine-conjugated PEPE	Convergent and divergent synthesis	~66%	~20%	–	0.4 μM (U 87MG and U 343 MGa)	Delivery of MTX across BBB and penetrate into the central necrotic regions	Dhanikula [77]

and the external surface of liposomes can be modified depending upon the development goal for each DDS type. For example, poly (ethylene glycol) (PEG), targeting ligands and/or antibodies are conjugated on the external surface of liposomes to improve the hydrophilicity, to enhance solubility during blood circulation and to provide passive and active targeting functions, eventually achieving a high drug efficacy with low toxicity. Liposomes are widely studied as one family of drug delivery carrier because of their biodegradability, biocompatibility, low toxicity and immunogenicity [30]. There are, however, some drawbacks in utilizing them for clinical applications, such as fast elimination from blood circulation and uptake by the reticulo-endothelial system (RES) [31,32]. In order to overcome those disadvantages, many researchers have been developing various liposomes reducing elimination rate by modifying the surface with PEG, as mentioned, to prevent non-specific binding and phagocytosis [33].

The low cellular influx of MTX molecules could be improved by encapsulating them in thermosensitive magnetoliposomes (TMs) containing magnetic γ-Fe_2O_3-glutamic acid made of 1,2-dipalmitoyl-sn-glycero-3-phosphocholine (DPPC) and cholesterol prepared by reverse-phase evaporation, as demonstrated by Zhu et al. [34]. The encapsulation efficiency (encapsulated drug/reacted drug) of MTX in the TM (MTX-TM) carrier was determined to be as high as ~61%. According to the pharmacokinetic behaviors of MTX-TM in a mouse model, the magnetic responsiveness in plasma and tissue was much more enhanced under a magnetic field (0.2 T) with twice maximum concentration (C_{max}) and 5 times area under the drug concentration–time curve (AUC) than those in the absence of a magnetic field. Even in skeletal muscle, a significant increase in C_{max} (3.85-folds) as well as AUC (9.68-folds) could be observed under a magnetic field, indicating that MTX-TMs could deliver MTX successfully to skeletal muscle tissues under an external magnetic field (Table 1) [34].

Microbubbles are a drug delivery carrier candidate, but their thin lipid or protein membranes may limit drug loading capacity (loaded drug/total DDS). To increase the loading capacity for anticancer drug molecules, an attempt was made to couple microbubbles with liposomes, taking advantage of ultrasound-mediated blood–brain barrier (BBB) crossing [35]. For example, MTX loaded biotinylated liposomes were first prepared with biotin-1,2-distearoyl-sn-glycero-3-phosphoethanolamine (DSPE)-polyethylene glycol (PEG) 2000, dipalmitoyl phosphatidyl-glycerol (DPPG), distearoyl phosphatidylcholine (DSPC), and PEG4000, and then biotinylated microbubbles were simply mixed and coupled with avidinylated microbubbles having a ~4.9 mg/mL loading capacity for MTX. According to the study on MTX delivery efficiency across the BBB in rats, MTX-liposome-coupled microbubbles exhibited high MTX concentration (25.3 ± 2.4 μg/g) in the parietal lobe after ultrasound application, which was 8.7-fold higher than that without ultrasound, and 3.6-fold higher than that of MTX itself without nanocarrier [36].

Pentak et al. reported the encapsulation of MTX and cytarabine (Ara-C) into a dipalmitoylphosphatidylcholine (DPPC)-based liposome. The encapsulation efficiency significantly increased up to 86.3% for Ara-C and 86% for MTX, respectively. However, the liposomal stability was fairly different depending on drug, since the drug-released amount from liposomes for Ara-C was ~1.8-fold greater than that for MTX on the first day and even after the 28th day [37].

Yang et al. prepared anisamide-functionalized reversibly cross-linked chimeric liposome (MTX-Anis-RCCP) through co-self-assembly of poly(ethylene glycol)-*b*-poly(N-2-hydroxypropyl methacrylamideg-lipoic acid)-*b*-poly(2-(dimethylamino)ethyl methacrylate) (PEG-P(HPMA-LA)-PDMA) and Anis-PEG-P(HPMA-LA)-PDMA followed by autocrosslinking in the presence of dithiothreitol (Fig. 4(A)). The MTX loading capacity of 65.1% in this liposome was found to be twice larger than that theoretically expected. In order to study the *in vivo* therapeutic effect of MTX-Anis-RCCP, samples with 15 mg MTX equiv. kg^{-1} were intravenously injected into H460 (lung carcinoma) tumor-bearing nude mice every three days (Fig. 4(B)). As shown in Fig. 4(C), MTX-Anis-RCCPs exhibited a significant inhibition effect on tumor growth without any change in body weight. According to the Kaplan-Meier survival curves, 100% survival rate was observed for the mice group treated with MTX-Anis-RCCPs after 45 days. Furthermore, the histological analyses of hematoxylin and eosin (H&E) stained sections of tumor and important organs revealed that apoptosis and necrosis occurred in tumor cells, but no significant damage was observed in major organs [38].

3.1.2. Polymeric nanoparticles

Polymeric nanoparticles for drug delivery applications have been extensively studied with natural and synthetic polymers used in various formulations. Usually, in polymeric nanoparticle desining, extra toxic cross-linking agents are needed for desired functions [39–41]. It has been, therefore, frequently attempted to synthesize polymeric nanoparticles without cross-linking agents on the basis of the self-association process. Kumar et al. reported pH-sensitive proteinoid polymeric nanoparticles that were prepared by a self-assembly process with acidic proteinoid Prot A7. Then MTX was encapsulated into the Prot A7 polymeric nanoparticles by simply mixing them directly, resulting in an encapsulation efficiency of 52%. From the release profile under simulated gastric conditions (pH 1.2), it became fairly clear that the MTX molecules were thermodynamically stable in the Prot A7 as evidenced by a small amount of MTX (7%) released in the first 2 h. On the other hand, 100% of MTX was released at neutral pH within 80 min. It was therefore, concluded that acidic proteinoid Prot A7 would be an excellent drug delivery nanocarrier for oral medications requiring specific functions such as pH-sensitive release and chemical stability under gastric conditions [42].

Several studies have also investigated introducing targeting moieties such as FA or peptides on polymeric nanoparticles for targeted drug delivery of MTX. Luteinizing hormone-releasing hormone (LHRH) was functionalized on human serum albumin (HSA) conjugated MTX by Taheri et al. and the resulting DDS (MTX-HSA-LHRH), was found to suppress viability of T47D (breast cancer) cell culture line. The IC_{50} (inhibitory concentration 50: the dose for 50% inhibition of growth) values for free MTX, MTX-HSA with and without LHRH on the T47D cell lines were 78.2, 49.2 and 5.82 nM, respectively. It was also understood that MTX-HSA functionalized with LHRH could specifically bind to the LHRH receptor in such a way that the MTX-HSA-LHRH particles could be internalized to the cell through receptor-mediated endocytosis. The FA are frequently used as an effective tumor-targeting agent due to its specific conjugation to folate receptors overexpressed in cancer cells [43]. Ji et al. reported FA conjugated chitosan (FA-CS) nanoparticles for targeted delivery of MTX (MTX/FA-CS). The release profiles for MTX from FA-CSs were influenced by the amount of encapsulated MTX. When the ratio of MTX/chitosan was 4/20, MTX release reached been 84%. On the other hand, MTX release was only 51% when the ratio was 1/20 [44]. Another study on FA modified chitosan nanoparticles (FA-CS-MTX) was reported by Beidokhti et al. The drug loading capacity and encapsulation efficiency of MTX was ~4.5% and 89.6%, respectively. According to *in vitro* test in human cervical HeLa cancer cell lines, FA-CS-MTX cell suppressed cancer cell viability twice than free MTX at drug concentration of 25 μg/mL after 48 h. However, no significant inhibition in cell proliferation could be observed for both drug only and DDS on the human gingival fibroblast HGF-1 cell culture line [45].

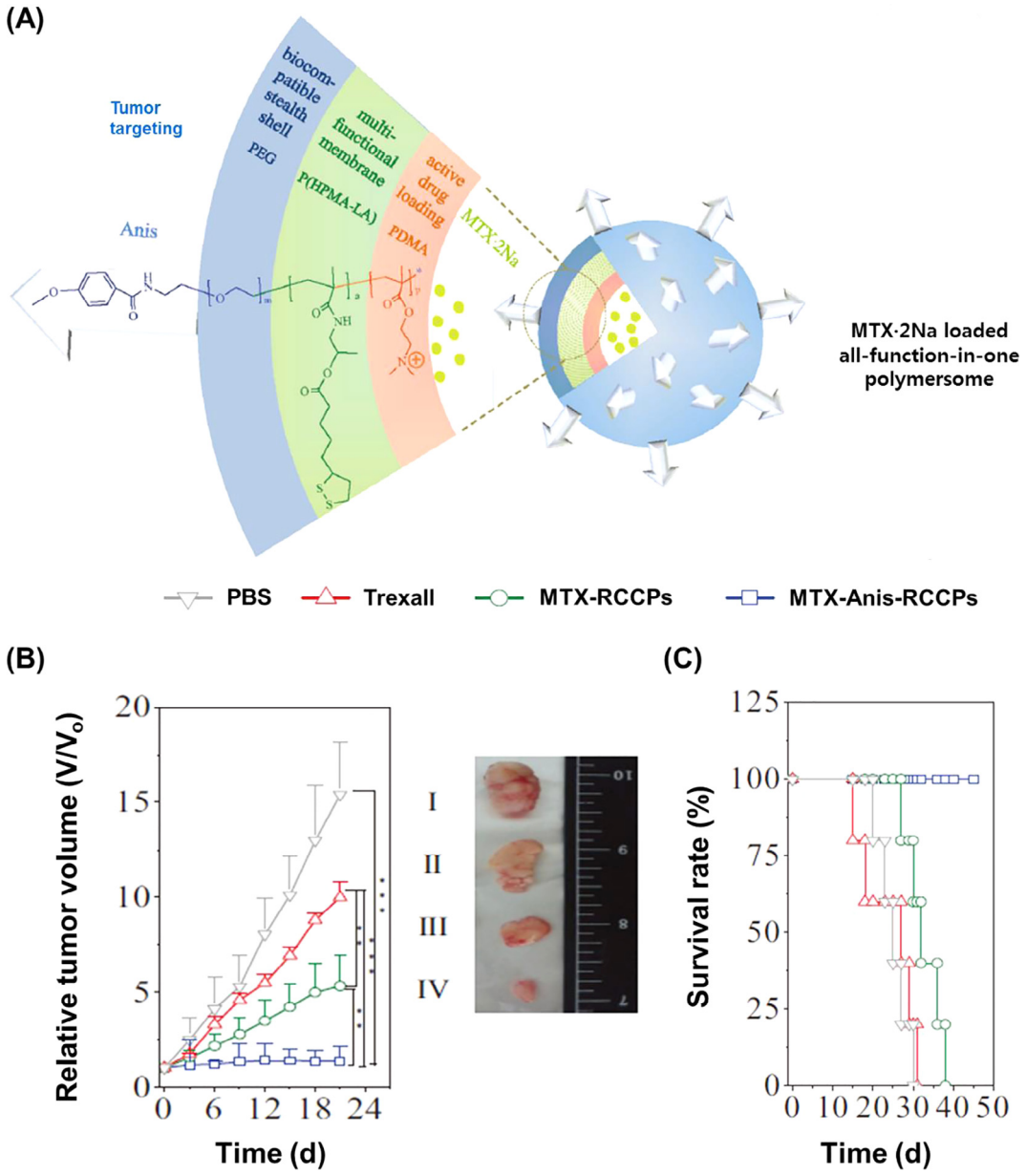

Fig. 4. (A) Structure and functions of Anis-RCCPs in targeted delivery of MTX·2Na to H460 human lung tumor-bearing nude mice. (B) H460 tumor growth inhibition by MTX-Anis-RCCPs. The drug was given on days 0, 3, 6, 9, and 12 at 15 mg MTX equiv. kg^{-1}. The inset shows photographs of tumor blocks excised on day 21 from mice treated with PBS (I), Trexall (II), MTX-RCCPs (III), and MTX-Anis-RCCPs (IV), respectively. And (C) Survival rates of mice following different treatments within 45 d. Data are presented as mean ± SD (n = 5). Reproduced from Ref. [38] with permission of WILEY-VCH Verlag GmbH & Co. KGaA, Weinheim.

Chen et al. studied PEGylated chitosan nanoparticles for MTX delivery (MTX-PEG-CS) (Fig. 5(A)) to overcome various drawbacks occurred in DDSs by enhancing drug stability, residence time during blood circulation, and by reducing PEG-protein immunogenicity [46,47]. The encapsulation efficiency of MTX in MTX-PEG-CS was determined to be 87.7%. As shown in Fig. 5(B), the cell viability of free MTX and MTX-PEG-CS was investigated in HeLa cell culture lines. After 24 h, MTX-PEG-CS (20 μM; MTX concentration) showed 49% inhibition of cell growth, while free MTX exhibited only 34% inhibition, indicating that PEG-CS had apparently played a role as a delivery nanocarrier [47].

In addition, polyamidoamine (PAMAM) has been widely studied as DDS carrier due to the easy particle size control and the surface functionalization. Leng et al. accomplished MTX delivery utilizing PAMAM dendrimers conjugated with chitosan nanoparticles (MTX-CS-PAMAM). The anticancer efficacy of MTX-CS-PAMAM and free MTX was evaluated in the A549 (adenocarcinomic human alveolar basal epithelial) cell culture line at various MTX concentrations (0.1, 0.2, 0.4, 0.8, 1.6 and 3.2 mg/mL). In this report, the IC_{50} values of free MTX and MTX-CS-PAMAM were determined to be 4.5 mg/mL and 0.8 mg/mL, respectively. Forty-eight percent cell death was observed at a free MTX concentration of 3.2 mg/mL, while higher cytotoxicity was seen for MTX-CS-PAMAM at low concentration (0.2 mg/mL) [48].

It is not easy to realize drug delivery brain tumors through the blood–brain barrier (BBB), and therefore, the mitigation of brain tumors is still a primary challenging research goal [49–51]. In a recent study, MTX was loaded into chitosan nanoparticles (MTX-CSNP) utilizing a spray drying method. The drug encapsulation efficiency was determined to be 90–93% depending on chitosan concentration. *In vivo* pharmacokinetic studies exhibited higher AUC values in brain for MTX-CSNP (25.18 μg·min/g) than free MTX

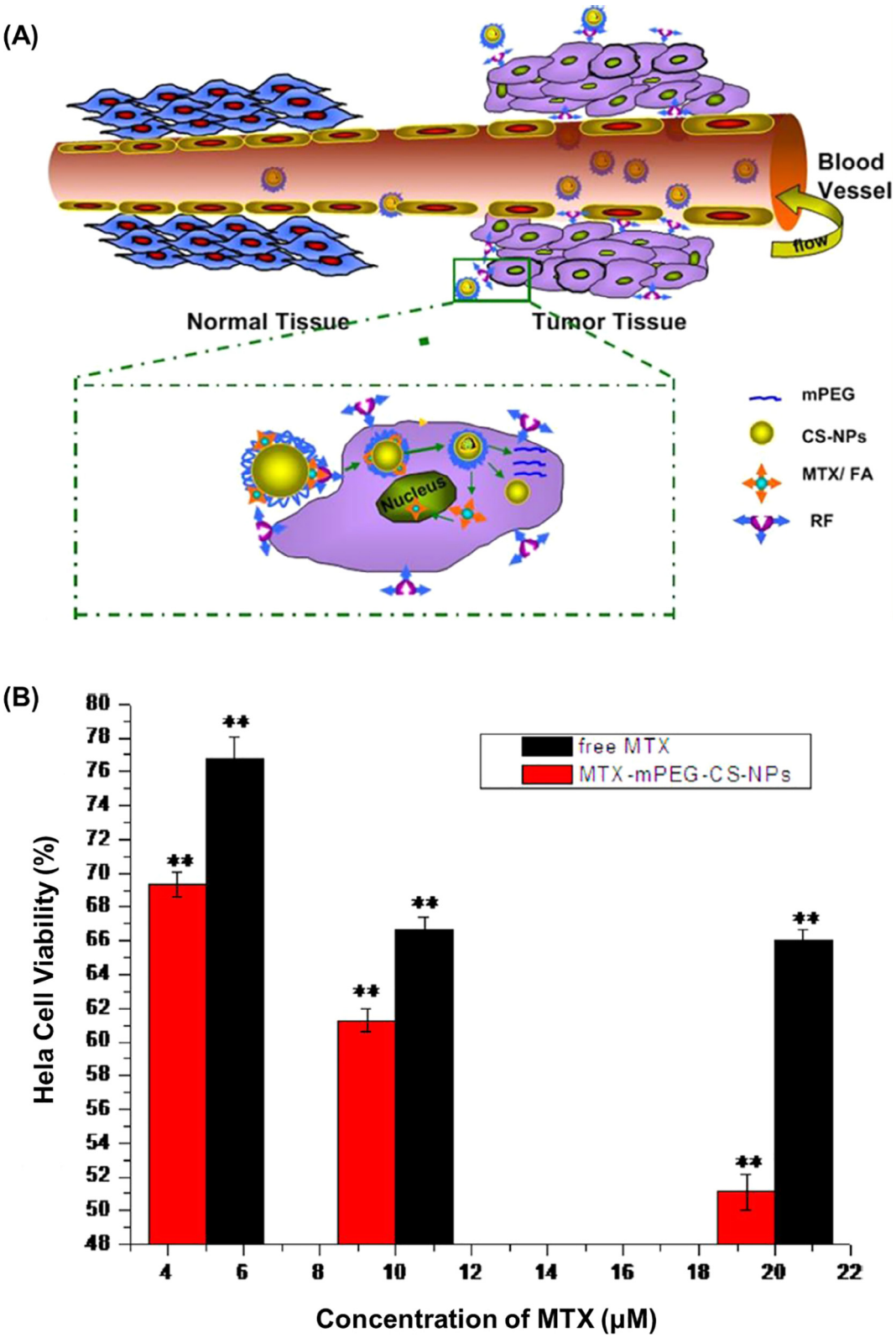

Fig. 5. (A) Schematic illustration of methotrexate (MTX) nanoparticles based on chitosan (CS) and methoxypoly(ethyleneglycol) (mPEG) for cancer nanotherapeutics. (B) Viability of HeLa cells treated with MTX (black) and MTX-mPEG-CS NPs (red) at various concentrations for 24 h (n = 3, $^{**}p < 0.01$). Reproduced from Ref. [47] with permission of American Chemical Society.

(21.19 μg·min/g). The paper also indicated that intranasally-administrated MTX-CSNP showed higher brain uptake of MTX than an intranasally or intravenously administrated MTX [52]. Kesharwani et al. prepared nanoparticles of poly lactic-co-glycolic acid (PLGA) conjugated with positively charged bovine serum albumin (CBA) to bypass the BBB for brain tumor treatment. In the study, MTX was immobilized in PLGA nanoparticles (NP), and then the CBA was further conjugated by solvent diffusion technique

(CBA-MTX-NP). Encapsulation efficiency was determined to be 79.9% for MTX-NP and 71.3% for CBA-MTX-NP, respectively. In particular, a biodistribution study was made for both samples in a C7 glioma cell xenografted Balb/c mice model. The amounts of MTX in various organs such as liver, kidney, spleen and tumor were determined to be 11.5, 7.2, 7.0 and 51.7 μg/g for MTX-NP, and 9.2, 5.1, 5.6 and 112.7 μg/g for CBA-MTX-NP after 24 h. The CBA conjugation on MTX-NP is considered to enhance anticancer activity due to the targeted specificity to tumor tissues [53].

3.1.3. Solid lipid nanoparticles

Solid lipid nanoparticles have been studied as a new type of colloidal nanocarrier for intravenously administered DDS [54]. Due to their membrane stability, biodegradability, low toxicity and organic solvent free condition, lipid nanoparticles are advantageous as DDS nanocarriers [55]. Ruckmani et al. studied MTX-loaded solid lipid nanoparticles (MTX-SLN) consisting of stearic acid, soya lecithin and sodium taurodeoxycholate. The encapsulation efficiency of MTX-SLN was determined to be ~40% depending on the ratio of MTX:stearic acid:soya lecithin. *In vitro* studies showed that MTX was released from SLN in a controlled manner (48 μg/mL after 10 h) in mouse serum, while free MTX was dissolved quickly with a concentration of 65 μg/mL within 6 h. It is clear that the half-life (8.2 h) and the mean residence time (MRT) of 16 h for MTX in the body extended to 14.5 h and 24 h, respectively, when SLN was applied [56]. Porous silicon-based nanomaterials, which is attractive inorganic drug delivery carrier due to biocompatibility, high-drug-loading capacity and biodegradability [57,58], could be combined with solid lipid system. Liu et al. reported that MTX-loaded thermally hydrocarbonized porous silicon encapsulated within solid lipid nanoparticles (THCPSi-SLMCs) had been used for MTX delivery. For the preparation of solid lipid nanoparticles, microfluidic flow-focusing methods was applied utilizing stearic acid, egg phosphatidylcholine and Poloxamer 188 (P-188) as precursors. The prepared THCPSi and THCPSi-SLMCs showed ~17% and ~12.5% drug loading capacity, respectively. The time-dependent release profiles of MTX from THCPSi with or without SLMCs were examined at various pHs. A 50% release of MTX from THCPSi was observed at ~15, ~30, ~14 min with pHs of 1.2, 5.0 and 7.4, respectively, while 50% release from THCPSi-SLMCs was achieved at ~45, ~75 and ~50 min. According to the pH-dependent release tests, it is evident that solid lipid nanoparticles could delay drug release of porous silicon nanocarrier [59].

Abdelbary and Haider also studied MTX-loaded nanostructured solid lipid carriers (MTX-NLC) [60], which were prepared by a high-shear homogenization method ultrasonicating lipids (Imwitor and Neobee®) and surfactants (Cremophor RH40 and Pluronic F127). The encapsulation efficiency of prepared MTX-NLCs was 42–85% depending on the composition among Imwitor and Neobee®, Cremophor RH40 and Pluronic F127. The anticancer effects were evaluated in the DU-145 (human prostate cancer) and A2780 (human ovarian carcinoma) cell culture lines for 72 h. At an MTX drug concentration of 31.6 μM, MTX-NLC exhibited stronger inhibition of DU-145 cancer cell growth than MTX itself. In the case of the A2780 cell line, the IC_{50} value for MTX-NLC was 3-fold lower (0.013 μM) than MTX itself (0.039 μM). MTX-loaded solid lipid nanoparticles (MTX-SLN) self-assembled with poly(ε-caprolactone), sorbitan monostearate and caprylic/capric triglyceride were also designed for MTX delivery [60]. The MTX-SLN showed a substantial reduction in proinflammatory and T-cell-derived cytokines, TNF-α (tumor necrosis factor-α) and IL-6 (interleukin 6), in a concentration-dependent manner [60].

Ferreira et al. reported a topical drug application utilizing a solid lipid-based drug delivery carrier consisting of cetyl palmitate, Miglyol® 812 and polysorbate 80 for skin-related diseases. MTX-loaded solid lipid nanoparticles (MTX-NLCs) showed 83% of high encapsulation efficiency with enhanced colloidal stability over 3 months. The Apical-to-basolateral flux of MTX-NLCs was evaluated with HaCaT (aneuploid immortal keratinocyte) cell lines and compared with free MTX. The MTX flux out of MTX-NLCs significantly increased up to 2-fold compared with free MTX. This showed that solid lipid nanoparticles could also deliver drugs in the treatment of skin-related disorders [61].

As described above, PEGylation is a common tool to enhance biocompatibility and to control the release behavior of drug molecules from nanocarriers. Kakkar et al. reported PEGylated solid lipid nanoparticles (PSD) prepared with stearic acid, Tween-80, soya lecithin and Triton X-100 through the solvent diffusion method. Thus prepared PSDs showed 6–28% of drug loading capacity depending upon their composition and 51–70% of high encapsulation efficiency. From a hemolytic activity and *in vitro* cell line assay, PSDs were determined to be harmless not only to red blood cell membranes but also to normal cells at sub-millimolar concentrations, indicating the high biocompatibility of PSD. Furthermore, *in vivo* biodistribution results of radioisotope ^{99m}Tc labeled PSD exhibited significant high tumor uptake (tumor/muscle = ~3 and ~6, tumor/blood = ~0.9 and ~1.3 for free MTX and MTX-PSD, respectively) which could improve tumor accumulation of drugs (Fig. 6(A) and (B)) [62].

Garg et al. demonstrated MTX delivery with solid lipid nanoparticles coated with fucose, a lectin receptor targeting sugar molecule, in a breast cancer animal model. Fucose is a sugar moiety commonly utilized for lectin receptor targeting. The solid lipid nanoparticles containing MTX were synthesized by the hot micro-emulsion method (Fu-SLNs-MTX). The drug loading capacity and encapsulation efficiency of Fu-SLNs-MTX was 15.2% with an 84% encapsulation efficiency. According to an *ex vivo* cytotoxicity study of MCF-7 (human breast cancer) cell lines, Fu-SLNs-MTX showed higher anticancer effect compared to SLNs without fucose or free MTX. *In vivo* biodistribution studies have shown the tumor-to-organ ratio for Fu-SLNs-MTX was significantly higher (3.4 for liver, 6.8 for spleen, and 7.6 for kidney in 8 h) than that for SLNs-MTX (3.1 for liver, 4.0 for spleen and 4.0 kidney), implying that surface modification of SLNs-MTXs with fucose was a good strategy for developing an advanced DDS with tumor targeting functions [63].

3.1.4. Polymeric micelles

Polymeric micelles have been intensively studied as drug delivery carriers due to their stability and compatibility in biological systems [64,65]. Zhang et al. reported MTX loaded m-PEG-polylactide (PLA) polymeric micelles utilizing a dialysis method. Thus prepared hybrid (PELs) showed drug encapsulation efficiency of 17–47% which corresponded to loading capacity of 3.7–12.8%. An time dependent release of MTX from PELs showed that drug molecules could be released in sustained manner of which rate was controlled by the chain length of PLA possibly due to the strong interaction between MTX and PLA chains [66]. Chen et al. studied Pluronic mixed micelles loaded with MTX. In this study, pluronic P105 and F127 encapsulated MTX (F127/P105-MTX hybrid) through thin-film hydration method. The respective drug encapsulation efficiency and loading capacity of F127/P105-MTX were 96.75% and 9.58%, which was much higher than physically encapsulation (encapsulation efficiency of 85.21% and loading capacity of 2.88%). The *in vitro* anticancer effect and cellular uptake for free MTX, physical encapsulate and F127/P105-MTX hybrid were evaluated on four different cell culture lines including H-460 (lung cancer), A549, KB and KBv (human carcinoma). Among them, the hybrid showed significant anticancer effect as well as high cellular uptake in KBv compared with A549 cells. According to *in vivo* KBv mice model study (Fig. 6(C)), substantial tumor inhibition rate of 71.4% was observed for F127/P105-MTX without any

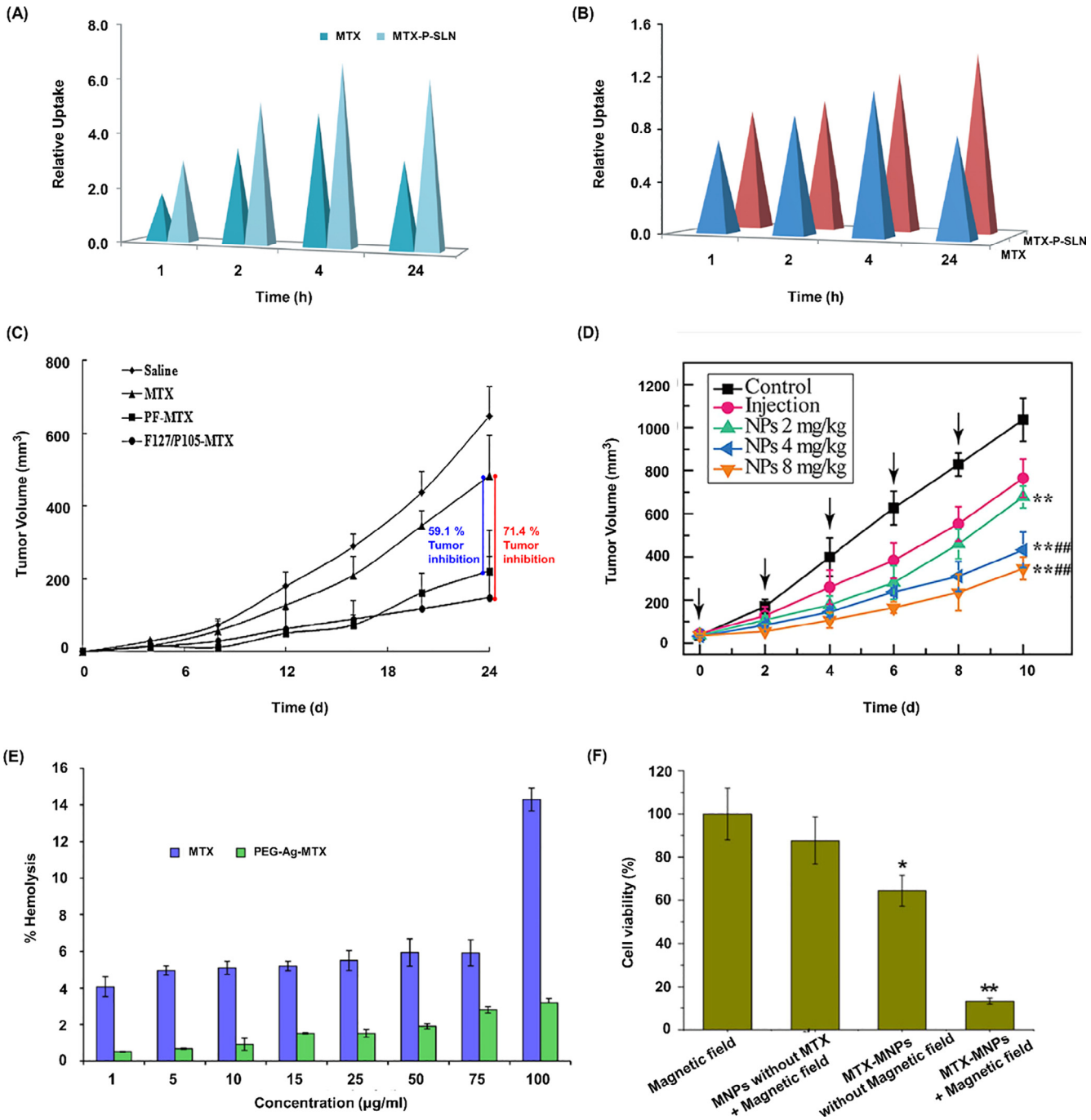

Fig. 6. (A) The relative uptake of ^{99m}Tc-MTX and ^{99m}Tc-M-P-SLNs in tumor: muscle and (B) tumor: blood, over a period of 24 h. Reproduced from Ref. [62] with permission of The Royal Society of Chemistry. (C) *In vivo* anti-tumor efficacy of F127/P105-MTX in subcutaneous KBv tumor-bearing mice. Each point represents average ± SD ($n = 6$). Reproduced from Ref. [67] with permission of Elsevier Ltd. (D) *In vivo* antitumor efficacy of MTX/PGD NPs delivered intravenous: tumor volume changes in 4T1-bearing BALB/c mice. For each animal, five consecutive doses were given (marked by arrows). Data represent mean ± SD ($n = 8$). $^{**}p < 0.001$ vs. saline control group, $^{\#\#}p < 0.001$ vs. MTX injection. Reproduced from Ref. [76] with permission of Nature Publishing Group. (E) Hemolysis of red blood cells. Reproduced from Ref. [87] with permission of Elsevier Ltd. (F) Influence of electromagnetic hyperthermia with MNPs, chemotherapy with MTX-MNPs without magnetic field, and their combination (electromagnetic hyperthermia with MTX-MNPs) on MCF-7 cell viability. The data are from three independent experiments ($^{*}p < 0.05$, $^{**}p < 0.01$ compared with magnetic field alone). Reproduced from Ref. [92] with permission of Springer.

serious loss of body weight, while the inhibition rate of physical encapsulates was only 59.1% [67].

Poly(aspatic-acid) derivative-based polymer micelles (PASPs) have various advantages as DDS nanocarrier such as low toxicity, biodegradability, biocompatibility, and low cost of preparation [68]. Jiang et al. reported PEG-coupled PASPs and evaluated their pharmacokinetic parameters in a mouse model. The biological half-time ($t_{1/2}$), AUC and total clearance (CL) of MTX-PEG-PASP were determined to be 2.39 h, 6.31 μg/mL·h and 19.0 mL/h, respectively. This result indicated that PEGylated polymer micelle delayed MTX clearance from blood circulation better than free MTX (1.01 h, 2.69 μg/mL·h and 44.8 mL/h, respectively) [69].

Polycaprolactone (PCL) has been shown to have excellent thermal and environmental stability and good enzymatic degradability [70]. The MTX-loaded diblock PCL micelle (PEG-b-BPCL) showed cumulative release profiles in the presence of esterase enzyme in

PBS (pH 7.4) with an IC_{50} value of 4 μg/mL, and cell death occurred mostly at a high concentration (10 μg/mL). As an another example of biocompatible polymer nanocarrier, soya lecithin (SL) from soya beans, known to be completely absorbed in the human body (above 90%) [71], was hybridized to form a PLGA-SL polymer micelle and was evaluated for MTX delivery in the MDA-MB-231 (breast cancer) cell culture line by Singh et al. The time dependent drug release and anticancer efficacy studies showed that MTX-PLGA-SL provided sustained release of MTX (~10%) at pH 7.4 with twofold reduced IC_{50} compared with free MTX. According to pharmacokinetic study, bioavailability was enhanced more than 4.9 times and half-life was increased to around 2.5 times after encapsulation with PLGA-SL [72].

Duan et al. reported dual responsive polymeric micelles consisting of cystaminedihydrochloride copolymer and PEG (PEG-CHO). The MTX loading efficiency was determined to be ~32% and the cumulative drug release rate was increased to 89% at pHs of 6.0 and 33% at pH 7.4, respectively. To evaluate *in vivo* tumor inhibition efficacy, free MTX and MTX-PEG-CHO were administered in an Ishikawa (endometrial adenocarcinoma) tumor-bearing mouse model. The tumor volume for the MTX-PEG-CHO-treated group increased by twofold (~34%) after 16 days, but compared with 0 day, that for the free MTX treated group was found to be 4-fold higher after 16 days [73].

3.1.5. Dendrimers

Dendrimers are multi-branched supramolecules not only with various functional groups on the surface but also with excellent drug conjugation properties [74]. An epidermal growth factor receptor (EGFR) targeting dendrimer nanocarrier was developed by Wu et al. MTX-loaded dendrimer DDSs were prepared with cetuximab (C225) and fifth-generation (G5) polyamidoamine. The cytotoxicity of free MTX and C225-MTX to $F98_{EGFR}$ (glioma) cells was evaluated on the basis of IC_{50} values of 0.42 nmol/L and 220 nmol/L, respectively, indicating that the latter was less toxic than the former. According to *in vivo* biodistribution study with the isotope iodine (^{131}I) in the $F98_{EGFR}$ and $F98_{WT\ (wild\ type)}$ xenografted mice models, the mean tumor radioactivity in mice for the C225-MTX treated group was 62.7 and 11.3 ID% (injected dose%) for $F98_{EGFR}$ and $F98_{WT}$, respectively, indicating the targeting function of EGFR ligand. The tumor-to-brain radioactivity of EGFR-positive gliomas was 10.8 with a 5.5-fold difference in retention of EGFR-positive versus EGFR-negative tumors after 24 h [75].

Zhao et al. reported an MTX-loaded co-dendrimer drug delivery carrier (MTX-PGD) with polyamidoamine (PAMAM) and oligoethylene glycols (OEG) synthesized via a classic dialysis method. The *in vitro* sustained drug release behavior of MTX-PGD was measured over 48 h and its kinetic properties showed an initial burst of ~40% followed by a slow release of ~60%, while almost 100% was released within 4 h for free MTX. *In vivo* test showed significant time-dependent tumor volume suppression by MTX-PGD (Fig. 6 (D)). Calculated tumor inhibition rates compared to the saline control were 44.8% and 78.5% for the free MTX and MTX-PGD, respectively, at the administration dose of 4 mg/kg [76].

One more example is a glucosamine-conjugated polyether-copolyester (PEPE)-based dendrimer as investigated by Dhanikula et al. Twenty percent of MTX molecules were loaded into a PEPE-dendrimer with a ~66% encapsulation efficiency. The IC_{50} value exhibited by the MTX-PEPE was ~0.4 μM, which was 1.5–5 times lower than free MTX (~2.4 μM) in U 87 MG (human primary glioblastoma) and U 343 MGa (human malignant glioma) cell lines. The transport efficiency of PEPE dendrimer across the BBB was evaluated with a rhodamine-labeled PEPE dendrimer and the glucosamine-conjugated PEPE showed 3.5 times higher transport efficiency than that without glucosamine [77].

3.2. Inorganic nanovehicles

3.2.1. Metal nanoparticles

Metal nanoparticles such as gold (AuNPs) and silver (AgNPs) were utilized as drug delivery vehicles due to their biocompatibility, functionalizable surfaces, easy binding with drug molecules and controllable sizes and shapes [78–80]. Chen et al. reported the *in vitro* cytotoxic effects and the *in vivo* antitumor effects of MTX-conjugated gold nanoparticles. MTX-AuNPs were prepared by a reduction of chloroauric acid with sodium citrate followed by MTX conjugation. The anticancer effect of MTX-AuNPs and free MTX were evaluated in the Lewis lung carcinoma (LL2) cell culture line. It was verified that the anticancer efficacy of MTX–AuNPs was significantly higher (more than 17-fold sensitive) for than free MTX in LL2 cell. According to this *in vivo* study, the tumor volume was significantly suppressed in the MTX–AuNP-treated mice group compared to the free MTX-treated or the PBS treated control [81].

The size and morphology of the nanocarrier are important parameters in delivery performance [82]. Tran et al. studied the size effect of AuNPs on a human choriocarcinoma (JAR) cell culture line at sizes of ~3 nm and ~ 20 nm. A 3-(4,5-dimethylthiazol-2-yl)-2,5-diphenyltetrazolium bromide (MTT) assay showed cell viability for smaller MTX-AuNPs was strongly suppressed (down to ~47%) while those for the larger size and free MTX were around ~70% and ~80%, respectively. According to the membrane damage test which is evaluated by the release amount of lactate dehydrogenase from cytosol, membrane damage by the small MTX-AuNPs (~69%) was approximately twice serious than that by large MTX-AuNPs (~36%). It was, therefore, concluded that the smaller the particle size, the more toxic MTX-AuNPs become [83]. Wang et al. reported the influence of MTX-AuNPs morphology on A549 cell lines. MTX-AuNPs with nanochains and nanoparticulate morpholgies were prepared by facile, one-pot, and hydrothermal methods. The MTX-AuNP nanochain changed to individual nanoparticle gradually by adding ethylene diamine tetra (methylene phosphonic acid) (EDTMPA) with different amounts. According to the cytotoxicity test on A549 cell lines by MTT assay, the individual MTX-AuNPs showed higher anticancer activity than MTX-AuNP nanochains. Furthermore, the MTX-AuNPs having equivalent drug loading capacity with MTX-AuNP nanochains showed better controlled drug release behavior and colloidal stability than the other [84].

To enhance AuNPs biocompatibility, Dey et al., utilized alginate and curcumin (Ccm) to prepare MTX conjugated AuNPs (MTX-Ccm-AuNPs) hybrid. The cell viability and cellular uptake of MTX-Ccm-AuNPs were evaluated in glioma (C6) and MCF-7 cell culture lines, exhibiting improved cellular uptake and anticancer activity compared with free MTX [85].

Redox and pH-sensitive AuNP based DDS was studied utilizing triple anticancer drugs including MTX, 6-mercaptopurine (MP) and doxorubicin (DOX), where co-conjugation of AuNPs and drugs (MTX-MP-DOX-AuNPs) was achieved by PEG block copolymer. Respective drug loading amount was ~49%, ~12% and ~43% for MTX, MP and Dox. An *in vitro* cell cytotoxicity test on various cancer cell lines (HeLa, MCF-7, A549 and human breast epithelial adenocarcinoma MDA-MB-231) proposed triple anticancer drug delivery by PEGylated AuNPs [86].

Muhammad et al. demonstrated the efficient anticancer activity and biocompatibility of PEG-capped MTX-AgNPs (PEG-MTX-AgNPs). PEG-MTX-AgNPs showed a ~40% encapsulation efficiency with higher anticancer activity; its IC_{50} value of 258.6 μg/ml was twice lower than that of free MTX (512.7 μg/ml). A hemolysis assay showed that the hemolytic activity of PEG-MTX-AgNPs was remarkably lower than that of free MTX (Fig. 6(E)), implying the blood compatibility of nanocarrier system [87].

3.2.2. Metal oxide nanoparticles

Metal oxides, especially iron oxide nanoparticles, have been considered as drug delivery carriers due to their spherical morphology with magnetic properties and large surface areas [88–90]. Furthermore, iron oxide magnetic nanoparticles (IONPs) were approved by the United States (US) Food and Drug Administration (FDA) as MRI contrast agents. In this regard, many attempts have been made to apply this magnetic oxide as a drug delivery vehicle with diagnostic functions. Kohler et al. synthesized MTX-conjugated IONPs (MTX-IONPs) by sequential modification of IONP's surface with (3-aminopropyl)-trimethoxysilane (APS) by silane coupling and MTX through peptization. According to the *in vitro* cellular uptake studies of MTX-IONPs in MCF-7, HeLa and rat cardiomyocyte cells, significantly higher amount of MTX-IONPs entered MCF-7 and HeLa cells compared with rat cardiomyocytes through folate receptor sites. The surprising thing in this study is that the covalently-bound MTX molecules on IONP surfaces remained unchanged until they were internalized into tumor cells, where they were cleaved by intracellular enzymes resulting in MTX release, which could minimize drug side effects to normal cells [91]. Gao et al. studied the thermochemotherapy and magnetic resonance imaging effects of MTX-conjugated IONPs. As shown in Fig. 6(F), the cytotoxicity assay results of MTX-IONPs on MCF-7 cell lines clearly showed that MTX-IONPs have excellent synchronous therapeutic effects not only due to MTX chemotherapy but also due to AC magnetic field-induced hyperthermia (13.3% and 64.5% of cell viability on MTX-IONPs with and without a magnetic field, respectively) [92].

According to the Corem-Slkmon's study on MTX-conjugated maghemite nanoparticles (MTX-MNPs) coated with human serum albumin (HSA) or PEG for convection-enhanced delivery (CED), MNPs could deliver MTX directly to the tumor tissues in brain by intracranial infusion. The *in vivo* biodistribution experimental results showed the distribution volume of HSA-coated MTX-MNPs was twice than uncoated MTX-MNP in rat brain, suggesting that MTX-MNPs are good candidates for CED treatment [93]. Kohler et al. also studied PEG-coated IONPs for improving particle stability in a solution by preventing particle agglomeration, and eventually enhancing particle uptake into target cells. Intracellular uptake results showed that PEG-coated MTX-IONPs were internalized into glioma cells (9L) cells in a concentration-dependent manner. Higher concentrations of PEG-coated MTX-IONPs (0.1 mg/mL) showed 8.0- to 9.0-fold higher cellular uptake than lower concentrations (0.01 mg/mL) after 2 h [94].

Li et al. reported hyperbranched PEG-grafted MTX-IONPs (HPG-MTX-IONPs) to enhance colloidal stability in an aqueous medium and bypassing elimination by macrophages. HPG-MTX-IONPs were prepared on the basis of sol–gel chemistry and thiol-ene click reaction, and the loading capacity of MTX was determined to be from 0.2% to 2% depending on the synthesis condition via an esterification reaction of hydroxyl groups of HPG with carboxylic acid groups of MTX. According to *in vitro* cellular uptake studies, HPG-MTX-IONPs showed ~5 times more uptake into KB cells compared with 3T3 fibroblasts and macrophages after 4 h. In addition, cytotoxicity results indicated that half of KB cells were dead upon treatment with HPG-MTX-IONPs, but no significant cytotoxicity could be seen for 3T3 fibroblasts and macrophages [95]. To improve therapeutic and imaging properties, Lin et al. prepared drug and Cy5.5 dye loaded system (Cy-MTX-PEG-CS-IONPs). The viability of HeLa was strongly reduced with Cy-MTX-PEG-CS-IONPs compared with free MTX. Plasma MTX concentration evaluated in animal model showed the blood circulation time of Cy-MTX-PEG-CS-IONPs was much more sustained than free MTX, with remarkably extended half life (3.6 h for Cy-MTX--PEG-CS-IONPs, 0.4 h for free MTX), higher AUC (18.3 mg·h/L for Cy-MTX-PEG-CS-IONPs, 4.3 mg·h/L for free MTX), longer MRT (4.4 h for Cy-MTX-PEG-CS-IONPs, 0.4 h for free MTX), and lower CL (0.2 L/h for Cy-MTX-PEG-CS-IONPs, 0.9 L/h for free MTX). The tumor growth was inhibited ~1.6 times by Cy-MTX-PEG-CS-IONPs compared to free MTX after 15 d [96].

3.2.3. Metal Salt nanoparticles

Calcium phosphate (CP) has been studied as bone cement owing to its easiness in forming porous structure, high biocompatibility, biodegradability in body fluid and osteoconductiveness [97,98]. Lebugle et al. investigated implantable calcium phosphate for the sustained release of MTX. The release kinetics of MTX-CPs were dependent on the loading amount of MTX in nanocarrier; the more MTX was loaded, the less portion of drug was release from the nanocarrier [99]. Li et al. investigated the *in vivo* effect of MTX-CP on osteogenesis with respect to resorption. First, MTX-CP was implanted to rabbit femoral condyle, where CP only without MTX was used as the control group. Although new bone volume (NBV) of MTX-CP (~2.1%) than that of CP only (~4.0%) in 1 month, the value becomes similar after 6 months (~38.0% and ~37.0% for CP and MTX-CP, respectively). It should be noted that, in systemic level, the MTX-CP preserved 55% of the payload drug after 30 days, implying the potential as sustained drug release in biological system. The results suggested that MTX-CP could be a suitable DDS not only for filling bone defects but also for controlling locally invasive bone tumors [100].

Calcium carbonate (CC) is one of the most widely studied biominerals for drug delivery because of its biodegradability and excellent biocompatibility, as well as its simple chemical composition [101]. However, the micrometer size limit of crystalline CC is a drawback for a drug delivery carrier [102]. Dai et al. investigated amorphous calcium carbonate nanoparticles (ACC) as drug delivery carriers for MTX. MTX-ACCs were prepared with a typical gas diffusion method at various pHs (pH 4.5, 7.2 and 8.5). An *in vitro* cell viability test was conducted with mouse adrenal pheochromocytoma (PC-12) and A549 cell culture lines at a drug concentration of 100 μg/mL after 24 h. The results showed that both CC and MTX-ACC had significantly high biocompatibility compared to free MTX in PC-12 cell lines. In the case of A549 cell lines, MTX-ACC showed the highest anticancer effects than CC for A549 cells after 24 h [103].

Dai et al. investigated silica-coated MTX-ACCs' core–shell structure (Si-MTX-ACCs) to improve the stability and protect core MTX-ACCs. The MTX-ACC core was synthesized under the different pH conditions, and then silica particles were subsequently decorated to form layers based on the well-known Stöber method. The anticancer efficiency of Si-MTX-ACCS were evaluated in PC-12 and A549 cell lines, and MTX-ACC with or without silica showed negligible cytotoxic effects, while the control groups exhibited fairly high toxicity in PC-12 cell lines. However, as with A549 cell lines, silica-coated MTX-ACCs showed enhanced anticancer effects compared to non-coated carriers [104].

3.2.4. Carbon nanomaterials

Carbon-based materials such as nanoparticles, nanotubes and graphenes have been intensively studied for various applications related to biological labeling, bioimaging, drug delivery and electronic applications [105–107]. Muthukuma et al. studied carbon nanoparticle (CP) coated with bovine serum albumin (BSA) and coupled with MTX on its surface (BSA-MTX-CP). The amount of MTX in BSA-MTX-CP was determined to be ~64%, and a ~79% MTX release from BSA-MTX-CP was achieved in a sustained manner in PBS at pH 7.4 after 48 h. Red blood cell (RBC) hemolysis and the MTT assay in A549 cell lines showed no significant RBC rupture up to 150 μg/ml, and the viability rate was as high as 90% even with the high concentration (150 μg/ml) of BSA-MTX-CPs [108]. Krishna et al. investigated digitonin (DG)-conjugated

MTX-CP for enhancing cellular uptake and cytotoxicity (DG-MTX-CP). The MTX encapsulation efficiency was estimated at ~94%, and the pH-dependent MTX release of DG-MTX-CP was around ~20% at pH 7.4 and ~81% at pH 5.0 over a period of 6 h. The viability of C6 cells upont drug administration was 81.4%, 78.6%, 77.0% and 71.6% at 12.5 mg/mL, 25 mg/mL, 37.5 mg/mL and 50 mg/mL of drug concentration while DG-MTX-CP showed 57.4%, 57.0%, 56.7% and 51.5% cell viability at corresponding drug concentration [109].

Carbon nanotubes (CNT) have various advantages as drug delivery carriers such as high surface area, chemically modifiable surfaces and high drug loading capacity, and photoacoustic effects as well [110,111]. Das et al. reported multiwalled CNT coated with fluorochrome (Alexa-fluor, AF488/647), radionuclide (^{99m}Tc), tumor-targeting ligand (FA), and an anticancer agent (MTX). The obtained IC_{50} values for MTX-CNT and free MTX were ~2.13 μg/mL and ~7.36 μg/mL in the A549 cell culture line, and 1.95 μg/mL and ~7.36 μg/mL in the MCF-7 line, respectively (Table 2). Through *in vivo* biodistribution profiles, the tumor-to-muscle ratio for free MTX and FA-MTX-CNT were calculated as 1.5 and 26.7, respectively, indicating that drug accumulation in the tumor was around 19.1 times higher for the latter than for the former, free MTX [112].

Graphenes have been widely utilized in academic and industrial fields due to their advantageous structural, electrical, thermal and mechanical properties. However, their surface chemical property like high hydrophobicity seemed to be an obstacle for use as DDSs due to easy formation of agglomerates [113]. An et al. attempted to overcome this disadvantage by hybridizing them with gelatin molecules having excellent biocompatibility, biodegradability and membrane forming function. The loaded MTX molecules were chemically bound with the gelatin reduced graphene oxide (gelatin-GO) via a π–π stacking interaction between aromatic portion of MTX and GO. Prepared MTX-gelatin-GO did not show any obvious cytotoxicity to A549 cells at an MTX concentration of 2 μg/mL and lower cytotoxicity compared with free MTX (70.2% and 68.4% for MTX-gelatin-GO and free MTX, respectively) after 48 h [114]. To improve GO biocompatibility, GO hydroxyethylation (HE-GO) was utilized as a carrier for MTX delivery by Du et al. The pH dependent *in vitro* release test showed the release rate of MTX from MTX-HE-GO reached ~50% at pH 5.5 and ~25% at pH 7.4 after 48 h. According to the cytotoxicity effect on A549 cell lines, the IC_{50} value of MTX-HE-GO was determined to be 50 ng/mL, which was significantly lower than the reported IC_{50} of MTX (7.4 μg/mL) [112,115].

In some cancer cells, such as human colon adenocarcinoma and breast cancer cells [116], dopamine (DA) receptors are overexpressed. To target DA sites, Masoudipour et al. prepared DA functionalized GO as an MTX delivery nanocarrier, and evaluated its anticancer activity on DA receptor overexpressed MCF-7 and DA receptor deficient HEK-293 (Human embryonic kidney) cell culture lines. The IC_{50} values for free MTX, MTX loaded GO and MTX-DA-GO on MCF-7 cells were 16.52 μg/mL, 18.8 μg/mL and 15.33 μg/mL, respectively. However, for HEK-293 cells, IC_{50} values of free MTX, MTX loaded GO and MTX-DA-GO were 73.18 μg/mL, 84.21 μg/mL and 83.73 μg/mL, respectively [117].

Shen et al. developed a MTX loaded GO-iron oxide (MNP) nanohybrid (GO-MNP) followed by several surface modification. The saturated loading amount of nanocarrier varied in the range of 256–896 mg/g depending on surface modification. The IC_{50} values of MTX-GO-MNP was approximately ~350 and 500 μg/mL in HepG2 and HeLa cells. This nanocarrier system could additionally take advantage of photothermal treatment due to MNP moiety, showing tumor volume suppression by ~58% upon near-infrared irradiation compared to controls (PBS treated) [118].

3.2.5. Porous nanoparticles

Mesoporous silica nanomaterials have also been suggested as a family of drug delivery carriers due to their well defined crystal structures and surface properties such as large specific surface areas and well-ordered channels with various geometries and narrow size distribution [119]. Carino et al. attempted to immobilize MTX molecules in MCM-41, a mesoporous silica nanomaterial. The amount of adsorbed MTX was determined to be around ~130 mg/g in MTX-Al-MCM-41 (MTX-aluminium containing MCM-41), when MTX was adsorbed inside the pores via a double soaking method in the presence of sodium buffer. The release profile for MTX out of MTX-Al-MCM-41 showed that mesoporous silica like MCM-41 might not be an excellent carrier for sustained release [120]. Vadia et al. reported that after formulating MTX with MCM-41 by changing some variables such as MTX concentration, MTX/MCM-41 ratio and stirring rate, MTX release of 60% in 10 min could be achieved, which is higher value than the market formulation of 26%. This is surely due to the fact that crystalline MTX was transformed to amorphous one with a reduced size upon encapsulation into MCM-41, which in turn improved drug solubility and as a consequence, enhanced dissolution rate [121].

Metal–organic frameworks (MOFs) consisting of organic ligands and metal ions could be a potential drug delivery carriers due to their diverse pore volumes, controllable pore windows, versatile functionality, bio-compatibility and high drug loading capacity [122–124]. Rowe et al. were successful in preparing gadolinium metal–organic framework (Gd-MOF) nanoparticles by reversible addition-fragmentation chain transfer (RAFT) polymerization, and in encapsulating MTX molecules into this MOF to form MTX-Gd-MOF. Its cancer cell suppression was studied in the canine hemangiosarcoma (FITZ-HSA) cell line, exhibiting dose-dependent anticancer efficacy [125]. In order to achieve pH responsive drug delivery function, Lin et al. prepared a hybrid drug by immobilizing MTX in a porphyrin-based MOF (MTX-PCN-221), and studied its cancer cell suppression ability in PC12 cells. The resulting hybrid drug exhibited higher cytotoxicity depending upon the loading concentration of MTX. However, the PC12 cells were still viable up to about 59%, even with a maximum dose of 100 μg/mL. The pH dependent drug release in this study was interesting; the amount of MTX release from MTX-PCN-221 was ~33% at pH 2.0, but ~100% at pH 7.4 after 72 h [126]. Lin et al. also demonstrated two types of MOFs with temperature responsiveness, including zinc-based MOFs (MTX-Zn-MOF and MTX-Zn-MOF-CH_3), which were prepared by solvothermal reactions. The absorbed amounts of MTX were ~13.5 by wt% for MTX-Zn-MOF and ~10.6 by wt% for MTX-Zn-MOF-CH_3 and the amount of MTX released from the former reached 54.5% after 72 h; only 23.1% of absorbed MTX was released from the latter at 37 °C. The release of MTX from two types of Zn-MOFs at 60 °C, was ~68% and ~24%, respectively, within 8 h [127].

3.2.6. Layered double hydroxides in nanoscale

For a decade, 2-dimensional (2D) inorganic materials, such as hydrotalcite-like compounds, have been applied in various industrial fields including flame retardants [128,129], catalysts [130–132]; however, their applicability are now expanded to biomedical fields [133,134]. With the fast advancement of nanotechnology and biotechnology, the convergence between them opened new ideas for 2D materials as biologically applicable multifunctional host matrices [135–138]. Among such 2D inorganic compounds, biocompatible layered double hydroxides (LDHs) are of great importance as drug delivery vehicles due to the current needs to develop advanced DDS, which is surely related to global issues such as the well-being and health care of human-beings, along with prolonged life, and overcoming diseases.

Table 2
Summary of inorganic nanocarriers for methotrexate delivery.

Nanocarrier	Materials	Synthetic method	Encapsulation efficiency	Loading capacity	Release of MTX	IC_{50} value	Achievement	Reference
Metal nanoparticle	Gold nanoparticle	Chemical reduction method	–	25%	70% (37 °C, pH 7.4, 11 h)	–	Enhanced controlled release and anticancer activity	Wang [84]
	Alginate, curcumin and gold nanoparticle	Thermal activation	–	1.3%	–	–	Dual drug molecule conjugated nanocarrier with two simple step	Dey [85]
	PEG and gold nanoparticle	In situ formation and stabilization	36.9%	11.53%	40% (37 °C, pH 7.4, 48 h)	–	Redox and pH dual responsible nanocarrier	Ghorbani [86]
	PEG and silver nanoparticle	Chemical reduction method	39.6%	–	–	258.6 μg/mL (MCF-7)	Lower hemolytic toxicity compared with free MTX	Muhammad [87]
Metal oxide nanoparticle	PEG and iron oxide	Sol–gel reaction	–	1.96%	–	–	Lower cytotoxicity on 3 T3 fibroblast and RAW macrophages	Li [95]
	Cy5.5, PEG, Chitosan and iron oxide	Chemical coprecipitation	–	6.2%	10% (37 °C, pH 7.4, 24 h)	–	Dual modal imaging and self-targeted drug delivery	Lin [96]
Metal Salt Nanoparticle	Calcium phosphate	Sol–gel reaction	–	6%	71.9% (37 °C, pH 7.4, 24 h)	–	Slow release system and suitable for bone implant	Lebugle [99]
	Calcium carbonate	Gas diffusion method	–	30.6%	60% (37 °C, pH 7.4, 60 h)	–	High drug loading capacity and anticancer activity	Dai [103]
Carbon Nanomaterial	Carbon nanoparticle and bovine serum albumin	Soot from cotton wick	–	64%	79% (37 °C, pH 7.4, 48 h)	–	High hemocompatibility and anticancer activity	Muthukuma [108]
	Carbon dot, digitonin	Injection of carbon precursor to hot noncoordinating solvents	94%	–	20% (37 °C, pH 7.4, 6 h)	–	Enhanced cytotoxicity to cancer cells and trace them with confocal microscope	Krishna [109]
	AF488/647, FA and 99Tc coated multiwalled CNT	Hydrolysable ester linkage (MTX)	86.4%	33.8%	10% (37 °C, pH 7.4, 48 h)	2.13 μg/mL (A549) 1.95 μg/mL (MCF-7)	Theragnostic application with high anticancer activity	Das [112]
	Gelatin, graphene oxide	Hummer's method	–	28.1%	40% (37 °C, pH 7.4, 12 h)	–	High colloidal stability with biocompatibility	An [114]
	Graphene oxide	Hummer's method	–	120%	25% (37 °C, pH 7.4, 48 h)	50 ng/mL (A549)	Enhanced water stability and controlled release	Du [115]
	Dopamine, graphene oxide	Hummer's method	81.8%	19.2%	80% (37 °C, pH 7.4, 24 h)	15.33 μg/mL (MCF-7) 83.73 μg/mL (HEK-293)	Sustained release and DA helps to target the nanocarrier to cancer cells	Masoudipour [117]
	Iron oxide and graphene oxide	Hummer's method	89.6%	–	49% (37 °C, pH 7.4, 40 h)	350 μg/mL (Hep G2) 500 μg/mL (HeLa)	Dual synergy of chemotherapy and photothermal therapy	Shen [118]
Porous Nanoparticle	MCM-41	Hydrothermal reaction	–	13%	42% (37 °C, pH 6.8, 2 h)	–	Controllable MTX release depending on Al	Carino [120]
	MCM-41	Hydrothermal reaction	–	48.8%	60% (37 °C, pH 1.2, 10 min)	–	Improvement of solubility of drug molecules and enhanced dissolution rate	Vadia [121]
	Porphyrin based MOF	Solvothermal reaction	–	40%	40% (37 °C, pH 2.0, 72 h)	–	High drug loading and sustained release without burst effect	Lin [126]
	Zinc based MOF	Solvothermal reaction	–	13.4%	54.5% (37 °C, pH 7.4, 72 h)	–	Temperature responsive drug release with thermal therapy	Lin [127]

To apply LDH for delivery vehicle, it is required to well define it chemically. The general formula of LDH can be described as $[M^{2+}_{1-x}M^{3+}_{x}(OH)_2]^{x+}(A^{n-})_{x/n} \cdot mH_2O$: M^{2+} = divalent metals such as Ca^{2+}, Mg^{2+}, Zn^{2+}, Ni^{2+}, etc. M^{3+} = trivalent metals such as Al^{3+}, and Fe^{3+}. A^{n-} = anionic species such as CO_3^{2-}, NO_3^-, Cl^-, and SO_4^{2-}, etc. ($0 < x < 1$). MgAl LDHs with CO_3^{2-} as an interlayer anion are already well known as anionic clay with the mineral name, hydrotalcite [139–142]. There are several examples of drug-LDHs with bioactive molecules, such as nucleotides [143–145], anticancer drugs [146,147], anti-inflammatory drugs [148], and vitamins [149,150]. All of them have been stabilized in the LDH interlayer space to form novel drug-LDH nanohybrids with various functions. Anion (drug) content in LDHs can easily be modified by controlling the ratio of M^{2+} to M^{3+} in the lattice, which is directly related to the magnitude of layer charge density and at the same time, that of anion exchange capacity. As shown in Fig. 7, various synthetic routes to drug-LDH nanohybrid materials, such as (A) co-precipitation, (B) ion-exchange, (C) calcination-reconstruction, and (D) exfoliation-reassembling are summarized [151].

The most attractive feature of LDH as a delivery vehicle is its partile size dependent cellular uptake behaviour. LDH nanoparticles smaller than ~250 nm can be permeabilized into cells through

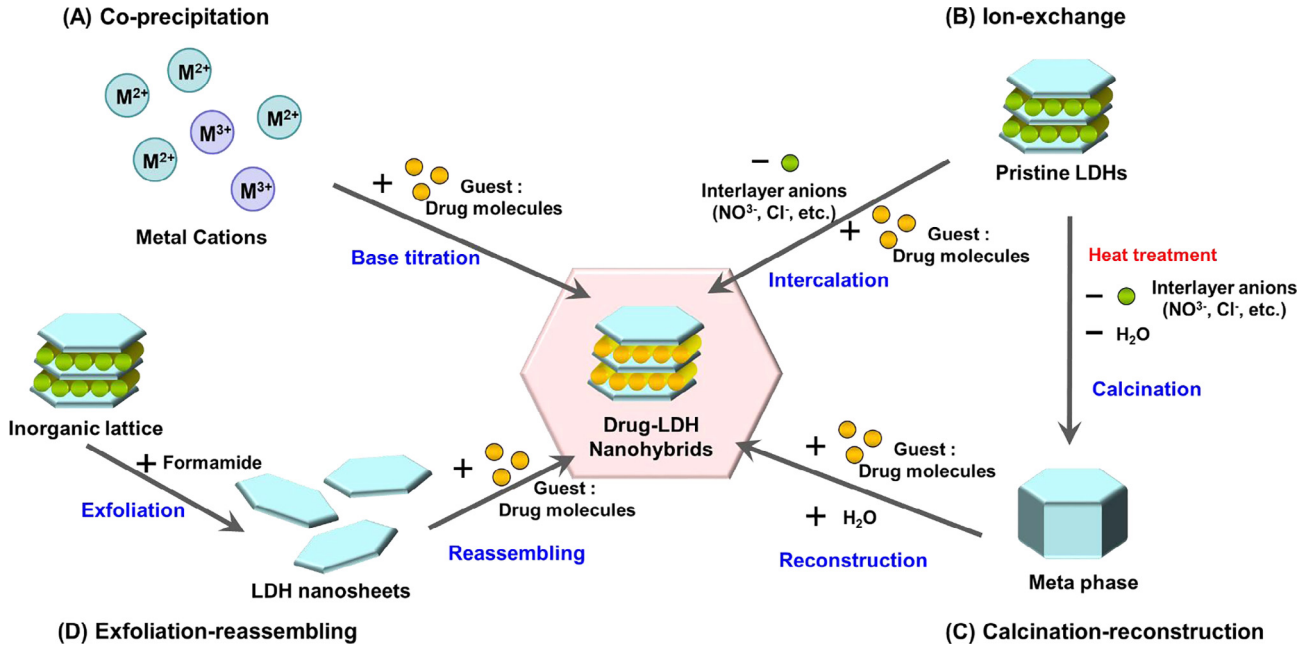

Fig. 7. Lattice engineering routes to intercalate drug molecules into two-dimensional (2D) LDH interlayer spaces: (A) coprecipitation, (B) ion exchange, (C) calcination-reconstruction, and (D) exfoliation-reassembling.

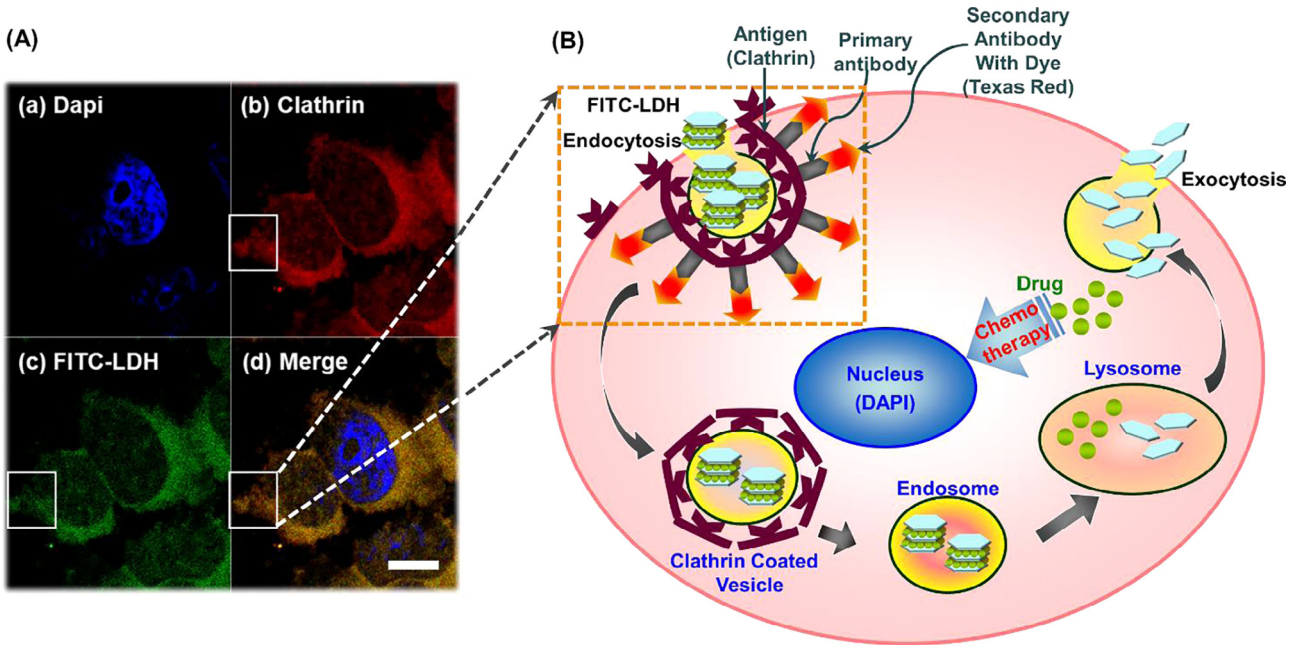

Fig. 8. Intercellular uptake mechanism of the LDH nanohybrids: (A) Confocal microscopy: co-localization of FITC-LDH and clathrin in MNNG/HOS cells. Localization of (a) the nucleus, (b) clathrin, and (c) FITC-LDH, the merged image (d) in MNNG/HOS cells. Cells were incubated with FITC-LDH for 2 h, treated with clathrin antibodies, and stained by TR and DAPI. Scale bar = 10 μm. Reproduced from Ref. [152] with permission of American Chemical Society. (B) Schematic illustration of the clathrin-mediated endocytosis.

clathrin-mediated endocytosis [152,153]. According to the immunofluorescence microscopy and confocal laser scanning microscopy studies on osteosarcoma cells (MNNG/HOS) treated with FITC-LDH (~100 nm), LDH nanoparticles were permeabilized into cells via clathrin-mediated endocytosis (Fig. 8). MNNG/HOS cells treated with FITC-LDH, a clathrin antibody and its secondary antibody conjugated with dye showed that FITC-LDHs were mainly present in the cytosol, and highly colocalized with the clathrin protein (Fig. 8(A)).

It is, therefore, suggested that the drug delivery with LDH can be a promising method for overcoming drug resistance of current anticancer agents thanks to clathrin-mediated endocytosis (Fig. 8 (B)) [154].

Recently, LDH nanoparticles with ~100 nm in size have been found to be biocompatible and targetable to tumor tissues and cells [152,153]. According to the MTT and trypan blue assays of MgAl-LDH and ZnAl-LDH in different cell lines such as normal and carcinoma cells, no significant effects on cell proliferation and viability up to 500 μg/ml could be seen for both nanoparticles, suggesting low cytotoxicity of LDH nanoparticles. The plasma membrane damage caused by LDH nanoparticles was also found to be negligible up to 100 μg/ml, but dose-dependent. In case of MgAl-LDH, a potent cytotoxicity was reported at high concentration (250–500 μg/ml) only in MCF-7 cells after 72 h. But such a high concentration of LDHs is not likely to be practically used in actual drug delivery systems. And the hemolytic potential is also an important toxicological factor to be examined in prior to the application of LDH nanoparticles for parenteral administration. When the LDH nanoparticles was incubated on isolated red blood cells, no hemolysis effect was induced at all the doses tested up to 100 μg/ml during 1–7 h incubation. After long incubation time (11–24 h), a small but negligible hemolysis effect (<2% for ZnAl-LDH and <1% for MgAl-LDH) could be observed [155–157].

As previously reported, not only the LDH nanovehicle but also the drug (MTX)-LDH and gene (siRNA)-LDH nanohybrids did not induce any liver toxicity or morphological abnormalities as confirmed by alanine aminotransferase (ALT) and aspartate aminotransferase (AST) levels in plasma and serum (Fig. 9(A)), and histopathologic analysis of hematoxylin-eosin (H&E) stained liver sections (Fig. 9(B) and (C)) [7,133]. It is, therefore, expected that LDH nanoparticles have a great potential for novel inorganic drug delivery carriers [155].

As shown in Table 3, many attempts have been made to develop LDH nanoparticles with targeting functions for chemotherapy.

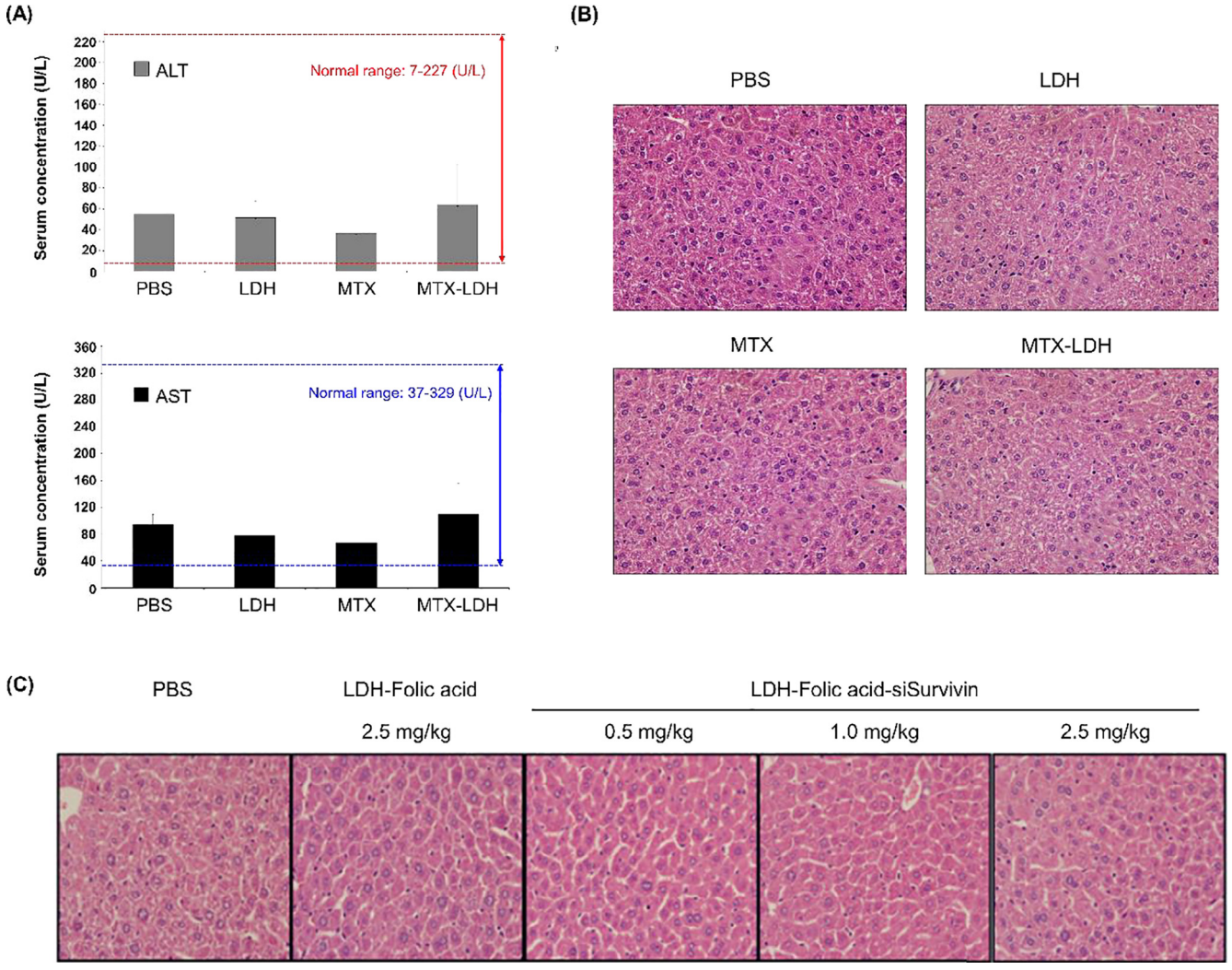

Fig. 9. Liver toxicity studies to assess liver damage and enzyme function after drug treatment. MTX-LDH nanohybrid system: (A) Aspartate aminotransferase (AST) and alanine aminotransferase (ALT) levels, and (B) Hematoxylin and eosin (H & E) staining of liver tissues. Reproduced from Ref. [7] with permission of Nature Publishing Group. Gene(siRNA)-LDH nanohybrid system: (C) H&E staining of liver tissues performed at day 3 after treatment (original magnification: ×100). Reproduced from Ref. [133] with permission of WILEY-VCH Verlag GmbH & Co. KGaA, Weinheim.

According to Oh et al., a significant *in vitro* anticancer effect of MTX-LDH nanohybrids was observed, surely due to an enhanced uptake of LDH particles into bone cancer cell culture lines such as Saos-2 and MG-63. The cell viability for MTX was not changed much with respect to the concentration, even above of 5×10^{-3} μg/mL, but that for MTX-LDH was strongly reduced with respect to the concentration. Such a difference in cell viability could be explained by the fact that MTX-LDH hybrid drug could permeate through cell membranes much more effectively than MTX itself [12]. In addition, Kim et al. reported that intracellular amount of MTX in the MTX-LDH treated MCF-7 cells were determined to be considerably higher than that in the free MTX treated, indicating that LDH played a role as a delivery carrier not only by facilitating the drug internalization into MCF-7 cells, but also by sustaining the drug release from LDHs [158]. Furthermore, the drug efficacies of nanohybrid systems with MTX-LDH and 5-fluorouracil (5-Fu)-LDH were compared with that of free drugs, and the order of drug efficacy was found to be as follows: MTX-LDH > MTX > doxorubicin (Dox) > 5-Fu-LDH > 5-Fu in all cell lines. And the MTX-LDH nanohybrid could, therefore, be a potential chemotherapeutic agent due to its excellent efficacy. Interestingly, a high drug efficacy was observed in human liver carcinoma cells (Hep1) similar to that seen in human lung adenocarcinoma cells (A549) [159]. According to Choi et al., they were very successful in controlling MTX-LDH particle size (~100 nm) and in maintaining their colloidal stability when dispersed in various media such as distilled water, saline, phosphate buffered saline (PBS) and RPMI1640 cell culture media. They also suggested an ideal particle size of 100–200 nm for EPR effect [16]. As demonstrated by Oh, a duplex anticancer drug nanohybrid, MTX-5-Fu-LDH, prepared by reconstruction method, showed the excellent tumor inhibition effect in the human cervical adenocarcinoma cells (HeLa), when it was compared with other drug-LDH nanohybrids, as the following order: MTX-5-Fu-LDH > MTX-LDH ≈ (MTX-LDH + 5-Fu-LDH) > 5-Fu-LDH [160]. And Li's group also reported that MTX could be incorporated into LDHs using a reverse microemulsion method. One thing to note here is that the tumor suppression efficiency of MTX-LDHs was decreased with an increase in the ε (dispersion coefficient) value. It is, however, not that surprising that the anticancer efficacy of MTX-LDH hybrids is closely associated with the colloidal stability of nanohybrid particles at least in their study [161]. According to the Chen's study, the cell viability of MTX-LDH (MTX concentration of 0.46 μg/ml) was dramatically dropped down to ~30%, though that of intact LDH remained unchanged. It is worth noting that the viability of cancer cells in the MTX-LDH nanoparticles treated group (only 0.05 μg/ml MTX) was lower than that of cells in the free MTX treated one (2 μg/ml).

In order to give active targeting function on LDH nanovehicle, the surface of LDH was modified with 3′-aminopropyl triethoxy silane (APTES) and further conjugated with FA through the coupling agent, 1-ethyl-3-(3-dimethylaminopropyl)carbodiimide (EDC). And thus prepared FA-LDH loaded with MTX showed a significant suppression in cancer cell growth [162].

As shown in Table 4, there has been several approaches to develop new nanoscale DDSs of MTX-LDH nanoparticles with targeting functions in *in vivo*. As demonstrated by the *in vivo* study with HOS-bearing mouse model, anti-tumor effects of free MTX and MTX-LDH were systematically evaluated [146], where 48 mice

Table 3
In vitro studies of MTX-LDH nanohybrids.

Metal composition of LDHs	Synthetic method for MTX-LDH	Particle size [nm]	Cell line	Challenges and achievements	Reference
Mg, Al	Co-precipitation	127 ± 25	• Human osteosarcoma cells (MNNG/HOS cell)	• The IC_{50} value of MTX-LDH in the cells was about 2.5-fold lower than that of MTX alone • MTX-LDHs penetrate the cell membrane more effectively than MTX only	Oh [152]
Mg, Al	Anion exchange	100–150	• Human osteosarcoma cells (Saos-2, MG-63)	• The nontoxic effects of LDHs for Saos-2 and MG-63 cells confirmed that the high anticancer effect of MTX-LDH nanohybrids was due to enhanced uptake by LDHs	Oh [12]
Mg, Al	Co-precipitation	100–150	• Human breast adenocarcinoma cells (MCF-7)	• Intracellular amount of MTX in MTX-LDH treated cells was considerably higher than that in free MTX treated cells, indicating LDH efficacy as a delivery carrier, which means that LDH can facilitate not only the internalization of drug molecules into cells, but also the controlled release of drugs from LDH	Kim [158]
Mg, Al	Co-precipitation	80	• Human lung adenocarcinoma cells (A549) • Human liver carcinoma cells (Hep1) • Human osteosarcoma cells (HOS)	• The efficacy of drug-LDH nanohybrids was compared with that of free drugs. MTX-LDH was the most effective in the following order: MTX-LDH > MTX > Dox > 5-Fu-LDH > 5-Fu in all cell lines • This indicated not only the high efficacy of drug-LDH nanohybrids, but also the great potential of MTX-LDH as a cancer chemotherapy agent • Interestingly, a high drug efficacy was observed in Hep1 cells similar to that seen in A549 cells	Choi [159]
Mg, Al	Co-precipitation	100	• Human osteosarcoma cells (Saos-2)	• It is worthy to note that the particle size of MTX-LDHs (~100 nm) was maintained when they were dispersed in various media; a particle size around 100–200 nm was optimum for cellular uptake and retention	Choi [16]
Mg, Al	Calcination-reconstruction	230	• Human cervical adenocarcinoma cells (HeLa)	• Anticancer drugs, MTX and 5-FU, and their combination, were incorporated into LDH by a reconstruction method • The MTX-5-Fu-LDH nanohybrid showed the highest inhibition efficacy in cancer cells in the following order: MTX-5-Fu-LDH > MTX-LDH ≈ (MTX-LDH + 5-Fu-LDH) > 5-Fu-LDH. This demonstrated that MTX-5-Fu-LDH was effective in a carrier dose-dependent manner	Kim [160]
Mg, Al	Reverse microemulsion method	84–114	• Human lung adenocarcinoma cells (A549)	• MTX-LDHs had higher tumor suppression efficiency compared to MTX alone	Liu [161]
Mg, Al	Co-precipitation	200	• Human cervical adenocarcinoma cells (HeLa) • Human carcinoma cells (KB)	• Folic acid-conjugated LDH nanoparticles loaded with MTX performed much better at killing cancer cells compared to free MTX	Yan [162]

Table 4
In vivo studies of MTX-LDH nanohybrids.

Metal composition of LDHs	Synthetic method for MTX-LDH	Particle size [nm]	Cell line and animal model	Administration route and amount	Challenges and achievements	Reference
Mg, Al	Co-precipitation	100	• Human osteosarcoma cells (HOS) • Xenograft mice model	• Intravenous injection • MTX 30 mg/kg • MTX-LDH 75 mg/kg, corresponding to 30 mg/kg MTX	• LD_{50} values were estimated to be between 50 and 75 mg/kg for MTX and higher than 100 mg/kg for MTX-LDH. • Tumor growth was significantly inhibited in HOS-bearing mice treated with MTX-LDH compared to the control group	Choi [146]
Mg, Al	Co-precipitation	130	• MCF-7/mot breast cancer cells • Orthotopic mice model	• Intraperitoneal injection • MTX 10 mg/kg • MTX-LDH 22.2 mg/kg, corresponding to 10 mg/kg MTX	• MTX-LDH had an even stronger antitumor effect than MTX with a mean tumor volume of 627.8 mm^3, representing 81.4% and 74.3% reductions in tumor volume compared with the PBS group and the MTX group, respectively. • The tumor-to-liver ratio of MTX in the MTX-LDH-treated-group was 6-fold higher than that of the MTX-treated-group after drug treatment for 2 h	Choi [7]
Mg, Al	Co-precipitation	100	• Human cervical cancer cells (C33A) • Orthotopic mice model	• Intraperitoneal injection • MTX 50 mg/kg • MTX-LDH 120 mg/kg, corresponding to 50 mg/kg MTX	• The antitumor effect of MTX-LDH was determined to be much more significant than that of MTX only. This represented a reduction of 81.5% and 66.4% in tumor volume relative to the PBS and MTX groups, respectively • Mice treated with MTX-LDH showed 3.5-fold higher tumor-to-liver ratio and 5.0-fold higher tumor-to-blood ratio of MTX than those treated with free MTX	Choi [147]
Mg, Al	Anion exchange	180–250	• Human osteosarcoma cells (HOS) • Xenograft mice model	• Intravenous injection • MTX, PLGA-MTX, or PLGA- MTX-LDH, at an equivalent dose of 30 mg/kg MTX	• The antitumor effect of PLGA-MTX-LDH represented a reduction of 70% and 49% in tumor volume relative to the MTX and PLGA-MTX groups, respectively	Ray [164]

were divided into four groups: control (PBS buffer), LDH (45 mg/kg), free MTX (30 mg/kg), and MTX-LDH (75 mg/kg, equivalent dose of 30 mg/kg MTX), and the treatments were intravenously injected via tail vein into each group of mice on 0, 7, and 14 days. The tumor volume was effectively decreased in the MTX-LDH treated group. It should be noted that the same amount of MTX (30 mg/kg) was applied in both free MTX and MTX-LDH treatments, corresponding to approximately the LD_{20} values [146].

Most recently, the *in vivo* studies have been made for the MTX-LDH nanohybrid particularly in two different orthotopic tumor models, breast cancer and cervical one, respectively [7,147]. And for the first time, the LDH carrier was prepared in a colloidal form and used for injectable nanomedicine in the orthotopic model [7], which is thought to be clinically more pertinent and therefore more predictive to estimate drug toxicity and/or efficacy than the conventional xenograft ones [163].

By examining the antitumor activities and biodistributions, the *in vivo* toxicity was carefully evaluated after intraperitoneal (ip) injection of MTX-LDH into each orthotopic mice model. The MTX-LDH nanohybrid system exhibited remarkably high antitumor efficacy in both *in vivo* models, surely due to the EPR effect. As shown in Table 4, the therapeutic efficacy of MTX-LDH, compared to pure MTX, showed 74% and 66% reductions in tumor volume after drug administration in the orthotopic breast cancer model and the cervical one, respectively. Interestingly, the tumor-to-liver ratio of MTX-LDH was found to be 6-fold higher in the former model and 3.5-fold higher in the latter one, respectively, than that of pure MTX after ip injections. By considering the tumor-to-liver ratio, which could be considered as an essential indicator in terms of therapeutic efficacy and safety profile, its remarkable enhancement in the MTX-LDH treated group is a clear sign indicative of its high potential as a safe and effective systemic delivery system for chemotherapy [7,147].

Ray et al. reported the comparative pharmacokinetic and antitumour efficacy studies with MTX, MTX-PLGA, and MTX-PLGA-LDH nanoparticles in osteosarcoma-induced Balb/c nude mice *in vivo* model, and demonstrated clearly the superiority of MTX-PLGA-LDH, as a potential nanomedicine for chemotherapy, by comparing its efficacy with MTX-PLGA and free MTX [164].

4. Summary and perspectives

This review is focused on the therapeutic applications of nanocarrier-assisted MTX delivery systems with imaging and targeting functions for chemotherapy. At first, an effort was made to introduce a number of advanced drug delivery systems using nanovehicles such as liposomes, polymeric nanoparticles, solid lipid nanoparticles, polymeric micelles, dendrimers, metal nanoparticles, metal oxide nanoparticles, carbon nanomaterials and LDHs, and to understand their advantages and limitation in drug delivery applications. In general, organic vehicles can be easily prepared, controllable in size, and readily functionalized, but comparatively expensive and toxic due to the acidification upon degradation in body fluid. In case of inorganic nanovehicles, they also show controlled release, rich functionality, and targeted delivery, but there are still concerns due to the accumulation of inorganic nanoparticles in organs, when they were once internalized in the body. One exception to such a drawback is LDHs, since they are dissolvable and biodegradable in body fluid, different from other inorganic nanovehicles, and eventually very low in toxicity in terms of accumulation, circulation and metabolization.

And then attempts were mad to summarize their MTX hybrid drugs with what the research goal was in academia on the way of developing such advanced DDSs, and what the challenging issues and chances would be not only to overcome adverse effects of MTX, but also to enhance therapeutic efficacies by improving bioavailability and targeting functions with the aid of delivery vehicles.

MTX has been already well known as folate antagonists in terms of action mechanism. Their detailed interactions with biological system in chemotherapy, however, were not fully understood

due to unexpected adverse effects like toxicity, low cellular uptake, uncontrolled drug release, lack of specificity in both cellular and systemic level, drug resistance, difficulties in biological tracing and etc. Those issues in drug delivery research community will be overcome, step by step, by developing new advanced nanocarriers and performing fundamental studies, though they will be challenged again by the pharmaceutical market. Such advanced hybrid drug formulations based on DDS will surely provide chances, after accumulating more *in vivo* evidences, in the market, which is still dominated by conventional drug formulations with low price and cheap manufacturing costs.

As a matter of fact, various medical technologies based on nanoscience are being investigated competitively in laboratory level both academically and industrially, and all those experimental findings will surely contribute to the final goal of overcoming disease.

Acknowledgements

This work was supported by the National Research Foundation of Korea (NRF) Grant funded by the Korean Government (MSIP) (No. 2005-0049412 and No. 2016R1D1A1A02937308).

References

[1] European technology platform on nanomedicine nanotechnology for health vision paper and basis for a strategic research agenda for nanomedicine 2005. http://cordis.europa.eu/nanotechnology/nanomedicine.htm/, 2017 (accessed 30 May 2017).
[2] J. Shi, A.R. Votruba, O.C. Farokhzad, R. Langer, Nano Lett. 10 (2010) 3223–3230.
[3] V. Wagner, A. Dullaart, A.K. Bock, A. Zweck, Nat. Biotechnol. 24 (2006) 1211–1217.
[4] W.T. Purcell, D.S. Ettinger, Curr. Oncol. Rep. 5 (2003) 114–125.
[5] S.S. Abolmaali, A.M. Tamaddon, R. Dinarvand, Cancer Chemother. Pharmacol. 71 (2013) 1115–1130.
[6] Z.A. Khan, R. Tripathi, B. Mishra, Expert Opin. Drug Deliv. 9 (2012) 151–169.
[7] G. Choi, O. Kwon, Y. Oh, C.O. Yun, J.H. Choy, Sci. Rep. 4 (2014) 4430.
[8] J.J. Killion, R. Radinsky, I.J. Fidler, Cancer Metastasis Rev. 17 (1998–1999) 279–284.
[9] L.K. Rahman, S.R. Chhabra, Med. Res. Rev. 8 (1988) 95–155.
[10] A. Vora, A. Riga, D. Dollimore, K. Alexander, J. Therm. Anal. Calorim. 75 (2004) 709–717.
[11] G.G. Kimmick, C. Cirrincione, D.B. Duggan, K. Bhalla, N. Robert, D. Berry, L. Norton, S. Lemke, I.C. Henderson, C. Hudis, E. Winer, Breast Cancer Res. Treat. 113 (2009) 479–490.
[12] J.M. Oh, M. Park, S.T. Kim, J.Y. Jung, Y.G. Kang, J.H. Choy, J. Phys. Chem. Solids 67 (2006) 1024–1027.
[13] A.G. Gilman, L.S. Goodman, A. Gilman, Chemotherapy of neoplastic diseases, in: L.L. Brunton (ed.), Macmillan, New York, USA, 2006.
[14] J.W. van der Heijden, B.A. Dijkmans, R.J. Scheper, G. Jansen, Nat. Clin. Pract. Rheumatol. 3 (2007) 26–34.
[15] J.J. McGuire, Curr. Pharm. Des. 9 (2003) 2593–2613.
[16] G. Choi, S.Y. Kim, J.M. Oh, J.H. Choy, J. Am. Ceram. Soc. 95 (2012) 2758–2765.
[17] R.M. Michaels, D.J. Nashel, A. Leonard, A.J. Sliwinski, S.J. Derbes, Arthritis Rheum. 25 (1982) 339–341.
[18] J.M. Kremer, J.K. Lee, Arthritis Rheum. 29 (1986) 822–831.
[19] J.R. Bertino, Cancer Res. 23 (1963) 1286–1306.
[20] J.M. Kremer, C.T. Phelps, Arthritis Rheum. 35 (1992) 138–145.
[21] R. Rau, B. Schleusser, G. Herborn, T. Karger, J. Rheumatol. 24 (1997) 1881–1889.
[22] S.K. MacKinnon, G. Starkebaum, R.F. Willkens, Semin. Arthritis Rheum. 15 (1985) 119–126.
[23] G.S. Alarcóan, I.C. Tracy, W.D. Blackburn Jr, Arthritis Rheum. 32 (1989) 671–676.
[24] M.E. Weinblatt, H. Kaplan, B.F. Germain, R.C. Merriman, S.D. Solomon, B. Wall, L. Anderson, S. Block, R. Small, F. Wolfe, J. Rheumatol. 18 (1991) 334–338.
[25] Y. Yazici, D. Erkan, S.A. Paget, J. Rheumatol. 29 (2002) 1586–1589.
[26] L.M. Buckley, C.A. Bullaboy, L. Leichtman, M. Marquez, Arthritis Rheum. 40 (1997) 971–973.
[27] D.E. Furst, J.M. Kremer, Arthritis Rheum. 31 (1988) 305–314.
[28] M.M. Gottesman, Annu. Rev. Med. 53 (2002) 615–627.
[29] A.D. Bangham, Chem. Phys. Lipids 64 (1993) 275–285.
[30] A.L. Klibanov, K. Maruyama, V.P. Torchilin, L. Huang, FEBS Lett. 268 (1990) 235–237.
[31] G. Batist, G. Ramakrishnan, C.S. Rao, A. Chandrasekharan, J. Gutheil, T. Guthrie, P. Shah, A. Khojasteh, M.K. Nair, K. Hoelzer, K. Tkaczuk, Y.C. Park, L. W. Lee, J. Clin. Oncol. 19 (2001) 1444–1454.
[32] L. Harris, G. Batist, R. Belt, D. Rovira, R. Navari, N. Azarnia, L. Welles, E. Winer, T.D.S. Group, Cancer 94 (2002) 25–36.
[33] G. Blume, G. Cevc, Biochim. Biophys. Acta 1146 (1993) 157–168.
[34] L. Zhu, Z. Huo, L. Wang, X. Tong, Y. Xiao, K. Ni, Int. J. Pharm. 370 (2009) 136–143.
[35] I. Lentacker, B. Geers, J. Demeester, S.C. De Smedt, N.N. Sanders, Mol. Ther. 18 (2010) 101–108.
[36] X. Wang, P. Liu, W. Yang, L. Li, P. Li, Z. Liu, Z. Zhuo, Y. Gao, Int. J. Nanomed. 9 (2014) 4899–4909.
[37] D. Pentak, V. Kozik, A. Bąk, P. Dybał, A. Sochanik, J. Jampilek, Molecules 21 (2016) E1689.
[38] W. Yang, Y. Zou, F. Meng, J. Zhang, R. Cheng, C. Deng, Z. Zhong, Adv. Mater. 28 (2016) 8234–8239.
[39] F. Forni, M.A. Vandelli, R. Cameroni, J. Microencapsul. 9 (1992) 29–39.
[40] B.C. Thanoo, M.C. Sunny, A. Jayakrishnan, J. Pharm. Pharmacol. 44 (1992) 283–286.
[41] M.C. Levy, M.C. Andry, J. Microencapsul. 8 (1991) 335–347.
[42] A.B.M. Kumar, K.P. Rao, Biomaterials 19 (1998) 725–732.
[43] A. Taheri, R. Dinarvand, F. Atyabi, F. Ahadi, F.S. Nouri, M.H. Ghahremani, S.N. Ostad, A.T. Borougeni, P. Mansoori, Int. J. Mol. Sci. 12 (2011) 4591–4608.
[44] J. Ji, D. Wu, L. Liu, J. Chen, Y. Xu, Polym. Bull. 68 (2012) 1707–1720.
[45] H.R.N. Beidokhti, R. Ghaffarzadegan, S. Mirzakhanlouei, L. Ghazizadeh, F.A. Dorkoosh, AAPS PharmSciTech 18 (2017) 115–129.
[46] G. Pasut, F.M. Veronese, Prog. Polym. Sci. 32 (2007) 933–961.
[47] J. Chen, L. Huang, H. Lai, C. Lu, M. Fang, Q. Zhang, X. Luo, Mol. Pharm. 11 (2014) 2213–2223.
[48] Z.H. Leng, Q.F. Zhuang, Y.C. Li, Z. He, Z. Chen, S.P. Huang, H.Y. Jia, J.W. Zhou, Y. Liu, L.B. Du, Carbohydr. Polym. 98 (2013) 1173–1178.
[49] Y.E.L. Koo, G.R. Reddy, M. Bhojani, R. Schneider, M.A. Philbert, A. Rehemtulla, B.D. Ross, R. Kopelman, Adv. Drug Deliv. Rev. 58 (2006) 1556–1577.
[50] N. Dwivedi, J. Shah, V. Mishra, M.C.I. Mohd Amin, A.K. Iyer, R.K. Tekade, P. Kesharwani, J. Biomater. Sci. Polym. Ed. 27 (2016) 557–580.
[51] A. Agarwal, U. Gupta, A. Asthana, N.K. Jain, Biomaterials 30 (2009) 3588–3596.
[52] Y. Sun, K. Shi, F. Wan, F.-D. Cui, J. Drug Deliv. Sci. Technol. 22 (2012) 167–174.
[53] P. Kesharwani, A. Jain, A. Jain, A.K. Jain, N.K. Garg, R.K. Tekade, T.R. Raj Singh, A.K. Iyer, RSC Adv. 6 (2016) 89040–89050.
[54] N.K. Jain, Advances in Controlled and Novel Drug Delivery, CBS Publishers & Distributors, New Delhi, India, 2008.
[55] R.H. Müller, S. Maaben, H. Weyhers, W. Mehnert, J. Drug Target. 4 (1996) 161–170.
[56] K. Ruckmani, M. Sivakumar, P.A. Ganeshkumar, J. Nanosci. Nanotechnol. 6 (2006) 2991–2995.
[57] H.A. Santos, L.M. Bimbo, V.P. Lehto, A.J. Airaksinen, J. Salonen, J. Hirvonen, Curr. Drug. Discov. Technol. 8 (2011) 228–249.
[58] L.M. Bimbo, O.V. Denisova, E. Mäkilä, M. Kaasalainen, J.K. De Brabander, J. Hirvonen, J. Salonen, L. Kakkola, D. Kainov, H.A. Santos, ACS Nano 7 (2013) 6884–6893.
[59] D. Liu, B. Herranz-Blanco, E. Mäkilä, L.R. Arriaga, S. Mirza, D.A. Weitz, N. Sandler, J. Salonen, J. Hirvonen, H.A. Santos, ACS Appl. Mater. Interfaces 5 (2013) 12127–12134.
[60] G. Abdelbary, M. Haider, Pharm. Dev. Technol. 18 (2013) 1159–1168.
[61] M. Ferreira, E. Silva, L. Barreiros, M.A. Segundo, S.A. Costa Lima, S. Reis, Int. J. Pharm. 512 (2016) 14–21.
[62] D. Kakkar, S. Dumoga, R. Kumar, K. Chuttani, A.K. Mishra, Med. Chem. Commun. 6 (2015) 1452–1463.
[63] N.K. Garg, B. Singh, A. Jain, P. Nirbhavane, R. Sharma, R.K. Tyagi, V. Kushwah, S. Jain, O.P. Katare, Colloid Surf. B-Biointerfaces 146 (2016) 114–126.
[64] R. Gref, Y. Minamitake, M.T. Peracchia, V. Trubetskoy, V. Torchilin, R. Langer, Science 263 (1994) 1600–1603.
[65] K. Kataoka, A. Harada, Y. Nagasaki, Adv. Drug Deliv. Rev. 47 (2001) 113–131.
[66] Y. Zhang, T. Jin, R.X. Zhuo, Colloid Surf. B-Biointerfaces 44 (2005) 104–109.
[67] Y. Chen, W. Zhang, J. Gu, Q. Ren, Z. Fan, W. Zhong, X. Fang, X. Sha, Int. J. Pharm. 452 (2013) 421–433.
[68] Y. Masayuki, M. Mizue, Y. Noriko, O. Teruo, S. Yasuhisa, K. Kazunori, I. Shohei, J. Control. Release 11 (1990) 269–278.
[69] T.Y. Jiang, Z.Y. Wang, C. Chen, F.K. Mo, Y.L. Xu, L.X. Tang, J.J. Liang, J. Appl. Polym. Sci. 101 (2006) 2871–2878.
[70] C. Jérôme, P. Lecomte, Adv. Drug Deliv. Rev. 60 (2008) 1056–1076.
[71] B. Surnar, M. Jayakannan, ACS Biomater. Sci. Eng. 2 (2016) 1926–1941.
[72] A. Singh, N. Thotakura, R. Kumar, B. Singh, G. Sharma, O.P. Katare, K. Raza, Int. J. Biol. Macromol. 95 (2017) 750–756.
[73] X. Duan, H. Chen, L. Fan, J. Kong, ACS Biomater. Sci. Eng. 2 (2016) 2347–2354.
[74] C.C. Lee, J.A. MacKay, J.M.J. Fréchet, F.C. Szoka, Nat. Biotechnol. 23 (2005) 1517–1526.
[75] G. Wu, R.F. Barth, W. Yang, S. Kawabata, L. Zhang, K. Green-Church, Mol. Cancer Ther. 5 (2006) 52–59.
[76] Y. Zhao, Y. Guo, R. Li, T. Wang, M. Han, C. Zhu, X. Wang, Sci. Rep. 6 (2016) 28983.
[77] R.S. Dhanikula, A. Argaw, J.F. Bouchard, P. Hildgen, Mol. Pharm. 5 (2008) 105–116.
[78] E.E. Connor, J. Mwamuka, A. Gole, C.J. Murphy, M.D. Wyatt, Small 1 (2005) 325–327.
[79] D.S. dos Santos, R.A. Alvarez-Puebla, O.N. Oliveira, R.F. Aroca, J. Mater. Chem. 15 (2005) 3045–3049.
[80] G. Palui, S. Ray, A. Banerjee, J. Mater. Chem. 19 (2009) 3457–3468.

[81] Y.H. Chen, C.Y. Tsai, P.Y. Huang, M.Y. Chang, P.C. Cheng, C.H. Chou, D.H. Chen, C.R. Wang, A.L. Shiau, C.L. Wu, Mol. Pharm. 4 (2007) 713–722.
[82] K.K. Sandhu, C.M. McIntosh, J.M. Simard, S.W. Smith, V.M. Rotello, Bioconjugate Chem. 13 (2002) 3–6.
[83] N.T.T. Tran, T.H. Wang, C.Y. Lin, Y. Tai, Biochem. Eng. J. 78 (2013) 175–180.
[84] W.Y. Wang, X.F. Zhao, X.H. Ju, Y. Wang, L. Wang, S.P. Li, X.D. Li, Int. J. Pharm. 515 (2016) 221–232.
[85] S. Dey, M.C.D. Sherly, M.R. Rekha, K. Sreenivasan, Carbohydr. Polym. 136 (2016) 71–80.
[86] M. Ghorbani, H. Hamishehkar, Int. J. Pharm. 520 (2017) 126–138.
[87] Z. Muhammad, A. Raza, S. Ghafoor, A. Naeem, S.S. Naz, S. Riaz, W. Ahmed, N.F. Rana, Eur. J. Pharm. Sci. 91 (2016) 251–255.
[88] A. Jordan, P. Wust, H. Fähling, W. John, A. Hinz, R. Felix, Int. J. Hyperthermia 25 (2009) 499–511.
[89] J. Ugelstad, L. Soderberg, A. Berge, J. Bergstrom, Nature 303 (1983) 95–96.
[90] R. Arshady, Biomaterials 14 (1993) 5–15.
[91] N. Kohler, C. Sun, J. Wang, M. Zhang, Langmuir 21 (2005) 8858–8864.
[92] F. Gao, Z. Yan, J. Zhou, Y. Cai, J. Tang, J. Nanopart. Res. 14 (2012) 1160.
[93] E. Corem-Salkmon, Z. Ram, D. Daniels, B. Perlstein, D. Last, S. Salomon, G. Tamar, R. Shneor, D. Guez, S. Margel, Y. Mardor, Int. J. Nanomed. 6 (2011) 1595–1602.
[94] N. Kohler, C. Sun, A. Fichtenholtz, J. Gunn, C. Fang, M. Zhang, Small 2 (2006) 172–785.
[95] M. Li, K.G. Neoh, R. Wang, B.Y. Zong, J.Y. Tan, E.T. Kang, Eur. J. Pharm. Sci. 48 (2013) 111–120.
[96] J. Lin, Y. Li, Y. Li, H. Wu, F. Yu, S. Zhou, L. Xie, F. Luo, C. Lin, Z. Hou, ACS Appl. Mater. Interfaces 7 (2015) (1920) 11908–11920.
[97] E.M. Ooms, E.A. Egglezos, J.G.C. Wolke, J.A. Jansen, Biomaterials 24 (2003) 749–757.
[98] R.P. del Real, E. Ooms, J.G.C. Wolke, M. Vallet-Regí, J.A. Jansen, J. Biomed. Mater. Res. Part A 65A (2003) 30–36.
[99] A. Lebugle, A. Rodrigues, P. Bonnevialle, J.J. Voigt, P. Canal, F. Rodriguez, Biomaterials 23 (2002) 3517–3522.
[100] D. Li, Z. Yang, X. Li, Z. Li, J. Li, J. Yang, Biomed. Mater. 5 (2010) 025007.
[101] L. Addadi, S. Raz, S. Weiner, Adv. Mater. 15 (2003) 959–970.
[102] G.B. Cai, G.X. Zhao, X.K. Wang, S.H. Yu, J. Phys. Chem. C 114 (2010) 12948–12954.
[103] C.F. Dai, W.Y. Wang, L. Wang, L. Zhou, S.P. Li, X.D. Li, Mater. Sci. Eng. C-Mater. Biol. Appl. 69 (2016) 577–583.
[104] C.F. Dai, W.Y. Wang, L. Wang, L. Zhou, S.P. Li, X.D. Li, RSC Adv. 6 (2016) 68335–68340.
[105] X. Yang, Y. Wang, X. Huang, Y. Ma, Y. Huang, R. Yang, H. Duan, Y. Chen, J. Mater. Chem. 21 (2011) 3448–3454.
[106] C. Wang, S. Ravi, U.S. Garapati, M. Das, M. Howell, J. Mallela, S. Alwarappan, S. S. Mohapatra, S. Mohapatra, J. Mater. Chem. B 1 (2013) 4396–4405.
[107] W. Chen, P. Yi, Y. Zhang, L. Zhang, Z. Deng, Z. Zhang, ACS Appl. Mater. Interfaces 3 (2011) 4085–4091.
[108] T. Muthukumar, S. Prabhavathi, M. Chamundeeswari, T.P. Sastry, Mater. Sci. Eng. C-Mater. Biol. Appl. 36 (2014) 14–19.
[109] A.S. Krishna, C. Radhakumary, S.S. Priya, R.M. Ramesan, K. Sreenivasan, RSC Adv. 6 (2016) 56313–56318.
[110] A. Bianco, K. Kostarelos, M. Prato, Expert Opin. Drug Deliv. 5 (2008) 331–342.
[111] G. Pastorin, Pharm. Res. 26 (2009) 746–769.
[112] M. Das, S.R. Datir, R.P. Singh, S. Jain, Mol. Pharm. 10 (2013) 2543–2557.
[113] D. Li, M.B. Muller, S. Gilje, R.B. Kaner, G.G. Wallace, Nat. Nanotechnol. 3 (2008) 101–105.
[114] J. An, Y. Gou, C. Yang, F. Hu, C. Wang, Mater. Sci. Eng. C-Mater. Biol. Appl. 33 (2013) 2827–2837.
[115] L. Du, S. Suo, D. Luo, H. Jia, Y. Sha, Y. Liu, J. Nanopart. Res. 15 (2013) 1708.
[116] P. Das, N.R. Jana, RSC Adv. 5 (2015) 33586–33594.
[117] E. Masoudipour, S. Kashanian, N. Maleki, Chem. Phys. Lett. 668 (2017) 56–63.
[118] J.M. Shen, F.Y. Gao, L.P. Guan, W. Su, Y.J. Yang, Q.R. Li, Z.C. Jin, RSC Adv. 4 (2014) 18473–18484.
[119] M. Vallet-Regi, A. Rámila, R.P. del Real, J. Pérez-Pariente, Chem. Mater. 13 (2001) 308–311.
[120] I.S. Carino, L. Pasqua, F. Testa, R. Aiello, F. Puoci, F. Iemma, N. Picci, Drug Deliv. 14 (2007) 491–495.
[121] N. Vadia, S. Rajput, Eur. J. Pharm. Sci. 45 (2012) 8–18.
[122] P. Horcajada, C. Serre, M. Vallet-Regí, M. Sebban, F. Taulelle, G. Férey, Angew. Chem. Int. Edit. 45 (2006) 5974–5978.
[123] J. Gao, J. Miao, P.Z. Li, W.Y. Teng, L. Yang, Y. Zhao, B. Liu, Q. Zhang, Chem. Commun. 50 (2014) 3786–3788.
[124] J. Gao, L. Bai, Q. Zhang, Y. Li, G. Rakesh, J.M. Lee, Y. Yang, Q. Zhang, Dalton Trans. 43 (2014) 2559–2565.
[125] M.D. Rowe, D.H. Thamm, S.L. Kraft, S.G. Boyes, Biomacromolecules 10 (2009) 983–993.
[126] W. Lin, Q. Hu, K. Jiang, Y. Yang, Y. Yang, Y. Cui, G. Qian, J. Solid State Chem. 237 (2016) 307–312.
[127] W. Lin, Q. Hu, J. Yu, K. Jiang, Y. Yang, S. Xiang, Y. Cui, Y. Yang, Z. Wang, G. Qian, ChemPlusChem 81 (2016) 804–810.
[128] J.H. Yang, W. Zhang, H. Ryu, J.H. Lee, D.H. Park, J.Y. Choi, A. Vinu, A.A. Elzatahry, J.H. Choy, J. Mater. Chem. A 3 (2015) 22730–22738.
[129] Q. Wang, X. Zhang, J. Zhu, Z. Guo, D. O'Hare, Chem. Commun. 48 (2012) 7450–7452.
[130] Y. Zhao, M. Wei, J. Lu, Z.L. Wang, X. Duan, ACS Nano 3 (2009) 4009–4016.
[131] Z. Lu, W. Xu, W. Zhu, Q. Yang, X. Lei, J. Liu, Y. Li, X. Sun, X. Duan, Chem. Commun. 50 (2014) 6479–6482.
[132] Y. Nie, Q. Yan, S. Chea, D. O'Hare, Q. Wang, Catal. Commun. 97 (2017) 47–50.
[133] D.H. Park, J. Cho, O.J. Kwon, C.O. Yun, J.H. Choy, Angew. Chem. Int. Ed. 55 (2016) 4582–4586.
[134] Z. Gu, B.E. Rolfe, A.C. Thomas, J.H. Campbell, G.Q. Lu, Z.P. Xu, Biomaterials 32 (2011) 7234–7240.
[135] M. Darder, M. López-Blanco, P. Aranda, F. Leroux, E. Ruiz-Hitzky, Chem. Mater. 17 (2005) 1969–1977.
[136] A.C.S. Alcântara, P. Aranda, M. Darder, E. Ruiz-Hitzky, J. Mater. Chem. 20 (2010) 9495–9504.
[137] M.A. Rocha, P.A.D. Petersen, E. Teixeira-Neto, H.M. Petrilli, F. Leroux, C. Taviot-Gueho, V.R.L. Constantino, RSC Adv. 6 (2016) 16419–16436.
[138] C. Chen, P. Gunawan, X.W. Lou, R. Xu, Adv. Funct. Mater. 22 (2012) 780–787.
[139] F. Cavani, F. Trifirò, A. Vaccari, Catal. Today 11 (1991) 173–203.
[140] G. Choi, H. Piao, M.H. Kim, J.H. Choy, Ind. Eng. Chem. Res. 55 (2016) 11211–11224.
[141] S. Miyata, Clays Clay Miner. 31 (1983) 305–3011.
[142] N. Iyi, T. Matsumoto, Y. Kaneko, K. Kitamura, Chem. Mater. 16 (2004) 2926–2932.
[143] J.H. Choy, S.Y. Kwak, J.S. Park, Y.J. Jeong, J. Portier, J. Am. Chem. Soc. 121 (1999) 1399–1400.
[144] J.H. Choy, S.Y. Kwak, Y.J. Jeong, J.S. Park, Angew. Chem., Int. Ed. 39 (2000) 4042–4045.
[145] L. Desigaux, M.B. Belkacem, P. Richard, J. Cellier, P. Leone, L. Cario, F. Leroux, C. Taviot-Gueho, B. Pitard, Nano Lett. 6 (2006) 199–204.
[146] S.J. Choi, J.M. Oh, H.E. Chung, S.H. Hong, I.H. Kim, J.H. Choy, Curr. Pharm. Des. 19 (2013) 7196–7202.
[147] G. Choi, H. Piao, Z.A. Alothman, A. Vinu, C.O. Yun, J.H. Choy, Int. J. Nanomed. 11 (2016) 337–348.
[148] L.N.M. Ribeiro, A.C.S. Alcântara, M. Darder, P. Aranda, F.M. Araújo-Moreira, E. Ruiz-Hitzky, Int. J. Pharm. 463 (2014) 1–9.
[149] J.H. Choy, Y.H. Son, Bull. Korean Chem. Soc. 25 (2004) 122–126.
[150] S. Aisawa, N. Higashiyama, S. Takahashi, H. Hirahara, D. Ikematsu, H. Kondo, H. Nakayama, E. Narita, Appl. Clay Sci. 35 (2007) 146–154.
[151] S.M. Paek, J.M. Oh, J.H. Choy, Chem. -Asian J. 6 (2011) 324–338.
[152] J.M. Oh, S.J. Choi, S.T. Kim, J.H. Choy, Bioconjugate Chem. 17 (2006) 1411–1417.
[153] J.M. Oh, S.J. Choi, G.E. Lee, J.E. Kim, J.H. Choy, Chem. Asian J. 4 (2009) 67–73.
[154] S.J. Choi, G. Choi, J.M. Oh, Y.J. Oh, M.C. Park, J.H. Choy, J. Mater. Chem. 20 (2010) 9463–9469.
[155] S.J. Choi, J.M. Oh, T. Park, J.H. Choy, J. Nanosci. Nanotechnol. 7 (2007) 4017–4020.
[156] S.J. Choi, J.H. Choy, Nanomedicine 6 (2011) 803–814.
[157] S.J. Choi, J.M. Oh, J.H. Choy, J. Inorg. Biochem. 103 (2009) 463–471.
[158] J.Y. Kim, S.J. Choi, J.M. Oh, T. Park, J.H. Choy, J. Nanosci. Nanotechnol. 7 (2007) 3700–3705.
[159] S.J. Choi, J.M. Oh, J.H. Choy, J. Phys. Chem. Solids 69 (2008) 1528–1532.
[160] T.H. Kim, G.J. Lee, J.H. Kang, H.J. Kim, T. Kim, J.M. Oh, Biomed Res. Int. 2014 (2014) 193401.
[161] Z.L. Liu, D.Y. Tian, S.P. Li, X.D. Li, T.H. Lu, Int. J. Pharm. 473 (2014) 414–425.
[162] L. Yan, W. Chen, X. Zhu, L. Huang, Z. Wang, G. Zhu, V.A.L. Roy, K.N. Yu, X. Chen, Chem. Commun. 49 (2013) 10938–10940.
[163] J.J. Killion, R. Radinsky, I.J. Fidler, Cancer Metastasis Rev. 17 (1998) 279–284.
[164] S. Ray, S. Saha, B. Sa, J. Chakraborty, Drug Deliv. Transl. Res. 7 (2017) 259–275.